scientific reports

Check for updates

OPEN

Identification biomarkers and therapeutic targets of disulfidptosis-related in rheumatoid arthritis via bioinformatics, molecular dynamics simulation, and experimental validation

Bin Xu[1]✉, Hai Long Zhang[1], Bo Shen[1], Jia Mei Wu[1], Meng Ting Shi[1], Xiao Duo Li[1]✉ & Qiong Guo[2]✉

The relationship between disulfidptosis and rheumatoid arthritis (RA) remains unclear. We aimed to identified biomarkers disulfidptosis-related in RA and revealed potential targeted drugs. Two microarray datasets (GSE93272, GSE45291) related to RA were downloaded from the Gene Expression Omnibus (GEO) database. Disulfidptosis-related genes(DRGs) were extracted from FerrDb database. GSE93272 was used to identify DRGs, and GSE45291 was used to verify results. Multivariate Cox regression analysis was used to identify candidate disulfidptosis-associated hub genes. The differentiated values of DRGs were determined by receiver operator characteristic (ROC) monofactor analysis to judge their potential quality as biomarkers. RT-qPCR were used to validate the expression of hub genes. Additionally, we analyzed the connection between the hub genes and the filtration of immune cells in RA. We made predictions about the miRNAs, TFs and possible drugs that regulate the hub genes. Subsequently, molecular docking was carried out to predict the combination of drugs with hub targets. Finally, molecular dynamics simulation was conducted to further verify the findings. Oxoacyl-ACP Synthase Mitochondrial(OXSM) was identified as a biomarker with high diagnostic value, and an RA diagnostic model based on OXSM for a single gene was constructed. The model showed high accuracy in distinguishing RA and healthy controls (AUC = 0.802) and was validated by external datasets, showing excellent diagnostic power (AUC = 0.982). Twelve potential drugs against RA were recognized by comparative toxicogenomics database (CTD). Molecular docking results showed that ICG 001 had the highest binding affinity to OXSM, and molecular dynamics simulations confirmed the stability of this complexes. Furthermore, CIBERSORT analysis showed a significant correlation between immune cell infiltration and OXSM, and a regulatory network of TFs-gene-miRNAs comprising 8 miRNAs and 34 TFs was identified. Finally, the RT-qPCR results showed that OXSM was significantly increased in the peripheral blood of RA patients compared with healthy controls, consistent with the bioinformatics analysis. These studies suggest that OXSM may be a potential biomarker and therapeutic target for diagnosing RA, and ICG 001 may be a potential drug for RA. These findings may provide new avenues for the effective diagnosis and treatment of RA.

Keywords Rheumatoid arthritis, Disulfidptosis, Bioinformatics, Molecular Docking, Molecular dynamics simulation

[1]Department of Clinical Laboratory, Anshun City People's Hospital, Guizhou 561000, China. [2]Anshun City Xixiu District Agriculture Bureau, Guizhou 561000, China. ✉email: binxu_ash@163.com; lxd19850704@163.com; guoqiong9292@163.com

Abbreviations

ACPA	anti-cyclic citrullinated peptide antibodies
ACTN4	Actinin Alpha 4
AS	ankylosing spondylitis
AUC	Area Under Curve
BP	Biological Process
CBFB	Core binding factor subunitβ
CC	Cellular Component
CTD	The Comparative Toxicogenomics Database
CUX1	Cut like homeobox 1
DEGs	Differentially expressed genes
DRGs	Disulfidptosis-related genes
EED	Embryonic Ectoderm Development
FEL	Free energy landscape
GEO	The Gene Expression Omnibus
GO	Gene Ontology Enrichment Analysis
GS	Gene significance
GSEA	Gene Set Enrichment Analysis
HSPD1	Heat shock protein D family member 1
JIA	juvenile idiopathic arthritis
KEGG	Kyoto Encyclopedia of Genes and Genomes
mAPK	mitogen-activated protein kinase
MF	Molecular Function
MM	Module membership
NOCA1	Non-centrosomal microtubule array protein 1
OSCC	Oral squamous cell carcinoma
OXSM	Oxoacyl-ACP Synthase Mitochondrial
PB	peripheral blood
PsA	psoriatic arthropathy
RA	Rheumatoid arthritis
RF	rheumatoid factor
Rg	Radius of gyration
RMSD	Root mean square deviation
RMSF	Root Mean Square Fluctuation
ROC	Receiver Operating Characteristic
ROS	reactive oxygen species
SASA	Solvent-accessible surface area
SPR	surface plasmon resonance
TAF 7	TATA-box binding protein associated factor 7
TFs	Transcription factors
WB	whole blood
WGCNA	Weighted gene co-expression network analysis
ZNF639	Zinc finger protein 639

Rheumatoid arthritis (RA) is a pathologically complexes autoimmune disease featured by inflammation and joint degeneration, often accompanied by persistent joint pain and gradual destruction of articular cartilage and bone, ultimately leading to severe dysfunction[1–4]. However, the pathogenesis of RA still needs to be fully understood. Disulfidptosis is a recently discovered new mode of cell death by the excessive accumulation of disulfides. It has been studied in cancer and other neurological diseases but has not been well described in rheumatoid arthritis. It has been shown that thiol-induced deterioration of the antioxidant defense system may lead to the pro-oxidant/antioxidant imbalance in RA[5], and chronic inflammation and oxidative stress are the main mechanisms in the pathophysiology of RA[6]. Some studies have shown that oxidative stress is linked to the progression of rheumatoid arthritis (RA) and its associated pathologies. When the function of the antioxidant defense system is impaired, or free radicals are overproduced, the body will enter an oxidative stress mode, thus inducing the apoptosis of chondrocytes[7–10], Excessive apoptosis of chondrocytes and altered cartilage degeneration are some of the leading causes of RA[11]. Excessive reactive oxygen species (ROS) play a vital role in the pathogenesis of RA[12]. In the physiological state, a moderate amount of ROS can promote immunity and repair and resist microbial infection. When ROS is excessive, it will induce severe oxidative stress and directly attack biological macromolecules such as proteins, nucleic acids, and lipids on the cell membrane and eventually lead to cell apoptosis, necrosis, and so on[9]. A large body of evidence shows that ROS leads to pathological changes in RA pathogenesis by affecting the damage of articular cartilage and chondrocytes[12], while CD4 + T cells, B cells, dendritic cells, mast cells and macrophages are also involved in RA pathogenesis[13], where neutrophils are considered to be the primary effector cells[14]. Neutrophils aggravate disease severity by excessive activation and release of reactive oxygen species ROS[15]. Moreover, increased cytokines such as TNF-α, IL-1, and IL-6 in patients with RA stimulate substantial production of ROS, leading to joint tissue destruction, which subsequently aggravates the disease[6,16]. In the inflamed RA joint cavity, the infiltration of monocytes and macrophages will continuously release high levels of ROS. The persistence of oxidative stress will induce apoptosis and activate immune cells, triggering the release of proinflammatory cytokines such as Th-17, exacerbating joint inflammation[17]. When insufficient or excessive depletion of NADPH is produced, intracellular redox homeostasis is disrupted[18], leading to excessive

intracellular accumulation of cystine, inducing disulfide bond stress in the actin cytoskeleton, and subsequent actin network collapse[19]. The actin cytoskeleton partly controls the phenotypic stability of chondrocytes, and chondrocytes maintain tissue homeostasis through a balance between synthesis and catabolism[20]. The collapse of the actin network and dysregulation of cartilage phenotypic stability lead to the destruction of chondrocytes and cartilage matrix, which then leads to irreversible chondrocyte damage and eventually induces RA[11,21]. Some studies have found that including decreased cytoskeletal proteins, decreased thiols, decreased glucose concentration, disulfide accumulation, osteoclast differentiation, and inflammatory cell infiltration in cartilage, synovium, and other tissues of RA patients[22–28]. Staron et al. noted that the concentration of thiol groups in the red blood cell membranes of RA patients was significantly reduced, possibly related to the aggregation of membrane proteins and an increase in disulfides[29,30]. Analysis of some studies showed a significant increase in cystine in the plasma of RA patients and a positive correlation between the severity of RA and increased cystine levels in the blood[6,25,26]. Excessive accumulation of intracellular cystine leads to disulfide bond stress and disulfidptosis[19]. It is, therefore, reasonable to assume that disulfidptosis may significantly affect the progression of RA.

Disulfidptosis is a newly discovered mode different from conventional programmed cell death. In the absence of glucose, a novel form of cell death resulting from disulfide stress caused by excessive cystine accumulation is called disulfidptosis[19]. Excessive accumulation of disulfide induces elevated levels of disulfide bonds between F-actin, leading to the disintegration of the actin network and, ultimately, cell death[19,31,32]. Induction or inhibition of specific cell death pathways has been used to treat various diseases, including autoimmune diseases[33,34]. The discovery of the disulfidptosis mechanism provides a new strategy for treating these diseases[19,31,32].

To better understand the regulatory mechanism of disulfide ptosis genes in RA, this study integrated bioinformatics, molecular docking, molecular dynamics simulation, and experimental verification to explore the role of disulfide ptosis genes in RA and provide new targets and potential drugs for its treatment. The workflow chart is shown in Fig. 1.

Materials and methods

Downloading and processing of the microarray data

Our study used the following screening criteria[35]: (1) all samples were collected from RA patients and healthy controls; (2) each group had a large sample size of more than 20 participants. In GSE93272, 275 whole blood samples were collected, comprising 232 from RA patients and 43 from healthy controls. GSE45291 included 493 RA samples and 20 healthy controls; (3) Test samples were sourced from human subjects; (4) the tissue used for sequencing was either whole blood (WB) or peripheral blood (PB). The samples in datasets GSE93272 and GSE45291 were obtained from blood samples of RA patients, and the consistent specimen source ensured the robustness of the subsequent analysis results. The expression profiles (GSE93272, GSE45291) related to RA were downloaded from the Gene Expression Omnibus (GEO)(https://www.ncbi.nlm.nih.gov/geo/)[36] and summarized in Table 1Dataset GSE93272[37]was used to screen hub genes, and dataset GSE45291[38] was used to verify the diagnostic relevance of hub genes.

Differential expression analysis

The R package limma[39](version 3.40.6)was used to identify differentially expressed genes (DEGs) between RA and healthy controls. The analysis included log2 transformation of the data, multiple linear regression using the lmFit function, and calculation of regulatory t-statistics, regulatory f-statistics, and log probability of differential expression using an empirical Bayes conditioning approach. Genes significantly different between RA and control groups were set with settings | logFC |> 1.2 and $p< 0.05$[40,41].

Differential gene enrichment analysis

The GO and KEGG[42] annotations of genes were extracted using the R package org.Hs.eg.db (version 3.1.0) and the KEGG REST API (https://www.kegg.jp/kegg/rest/keggapi.html), respectively. These annotations were used as the background, and the genes were mapped to the background set. GO and KEGG enrichment analyses were then performed using the R package clusterProfiler (version 3.14.3) to obtain the results of gene set enrichment[39,43]. The significance threshold was an adjusted P-value < 0.05[44].

Weighted gene co-expression network analysis

A scale-free co-expression network was constructed using the R package Weighted gene co-expression network analysis (WGCNA)[45]. The sensitivity was set to 3, and modules with a distance of less than 0.25 were merged to yield 16 modules with different colors. The correlation between each module and RA was then analyzed, and the most relevant module was selected for further analysis. Gene significance (GS) and module membership (MM) were calculated for each gene in the hub module, the threshold was set to MM > 0.8, and GS > 0.2, and potential RA-related genes were selected.

Disulfidptosis-related genes extraction

DRGs were retrieved from the FerrDb database's extended data[46], and duplicates were removed to extract effective targets.

Feature gene identification and GSEA analysis

The DRGs, DEGs, and WGCNA module genes were fed into Venny 2.1.0(http://bioinformatics.psb.ugent.be/webtools/Venn/) to identify overlapping targets. Two feature genes, OXSM and Actinin Alpha 4 (ACTN4), were obtained, and their expression levels were analyzed. Finally, the eigengenes' function and potential biological roles were further analyzed by Gene Set Enrichment Analysis(GSEA).

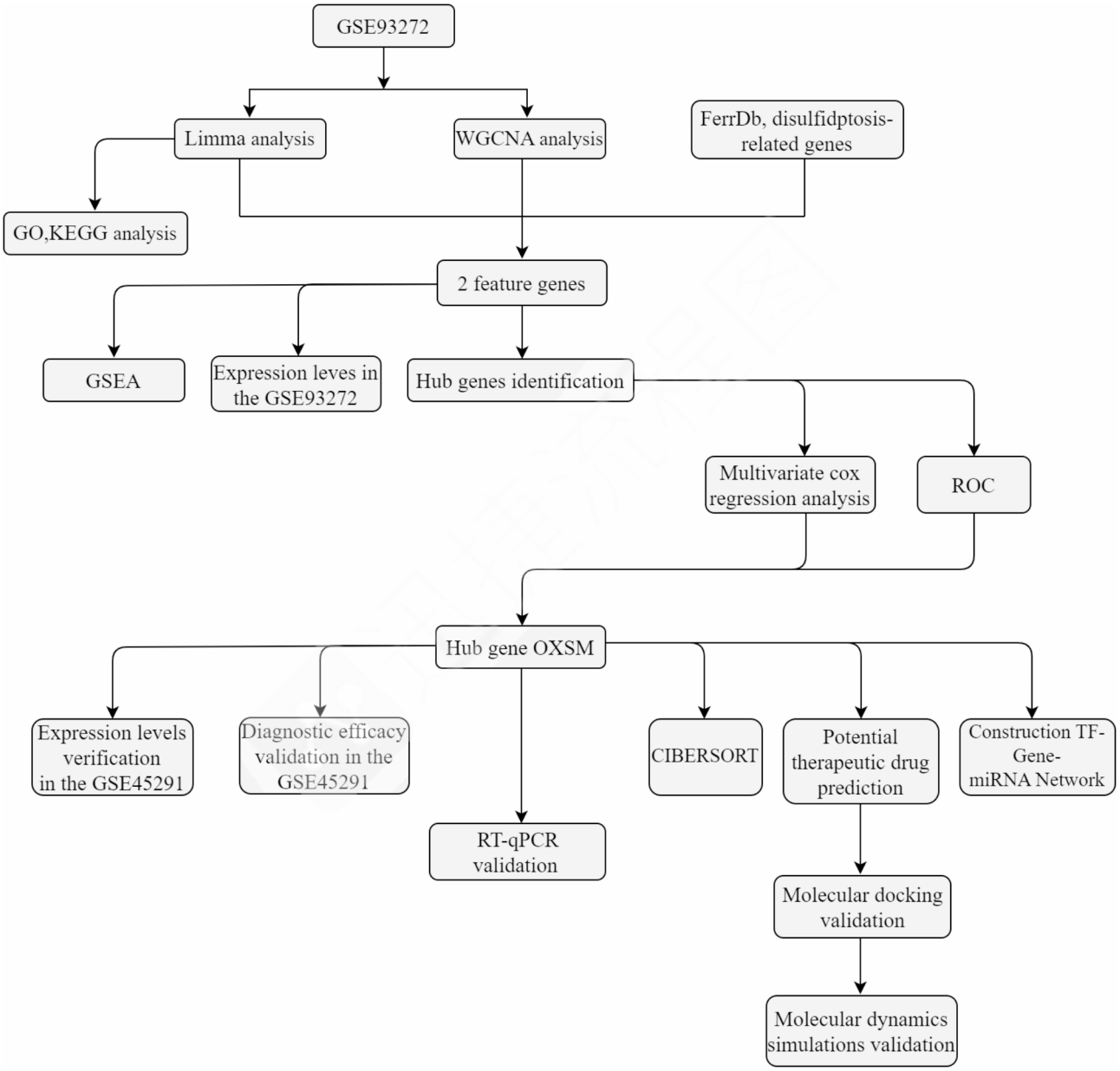

Fig. 1. Workflow diagram.

Data number	Platform information	RA group	Control group	Species
GSE93272	GPL570	232	43	*Homo sapiens*
GSE45291	GPL13158	493	20	*Homo sapiens*

Table 1. Descriptive statistics.

Hub gene identification, diagnostic model development and validation

To screen hub genes, we performed multivariate cox regression analysis[47] of the two characteristic genes. Further, the"pROC" R package was used to perform a receiver operating characteristic (ROC) monofactor analysis[48] on the training set GSE93272 and the validation set GSE45291, respectively, to judge the diagnostic value of the disulfidptosis-related biomarkers in RA patients. Normally, the closer the ROC curve is to the top left corner, the better the diagnostic performance[49], while the AUC (Area Under Curve) values range from 0.5 to 1, with values greater than 0.8 indicating good predictive accuracy and reliability in practice[50]. The filtering criteria of the hub genes were set at AUC > 0.800[51].

Immune infiltration analysis
CIBERSORT analyzed the relative proportions of the 22 immune cells in each sample[52,53], and bar plots showed the proportions of each immune cell type in the different samples. Furthermore, the correlation between the 22 infiltrating immune cells was analyzed using the Corrplot R package[54]. Boxplots compare the proportion of immune cells between RA and healthy controls and further analyze the correlation between hub genes and 22 immune cell types.

Construction of TFs-Gene-miRNAs network
Interactions between the TFs, miRNAs, and the hub genes were analyzed using the NetworkAnalyst3.0[55] and visualized with Cytoscape. Finally, we analyzed the correlation between TFs and OXSM in the GSE93272 dataset.

Potential therapeutic drug prediction
CTD is a publicly available database including 17,100 chemicals, 54,300 genes, 6100 phenotypes, 7270 diseases, and 202,000 exposure statements[56]. Potential drugs for OXSM prediction using CTD and demonstrating drugs - gene- diseases interactions via Sankey plots.

Molecular docking
The SDF format for all drugs were downloaded from the PubChem database (https://pubchem.ncbi.nlm.nih.gov/). PDB files for core proteins were obtained from the RCSB Protein Database (http://www.rcsb.org/), molecular docking by the online docking tool CB-Dock2[57], and visualized using PyMOL.

Molecular dynamics simulations
The Gromacs2023.2 program[58]performed molecular dynamics simulations[59,60]of 100ns[61–63]for small molecule-protein complexes. Calculating the binding free energy between ligand and receptor by MM/GBSA[64–67] provides detailed insights into the binding mode between small molecules and target proteins.

Quantitative realtime PCR
In this study, the peripheral blood of three healthy controls and five RA patients was used(our study is conducted in strict accordance with the Declaration of Helsinki.), and the total RNA was extracted using the column whole blood total RNA extraction and purification kit (Sangon Biotech, Shanghai, China). Reverse mRNA transcription was performed using the PrimeScript RT kit (TaKaRa, Dalian, China). RT-qPCR experiments were performed according to the instructions of SYBR Premix Ex Taq Kit (TaKaRa, Dalian, China) and performed on LightCycler 480 (Roche). GAPDH was used as the reference gene. Relative expression of genes was calculated via the $2^{-\Delta\Delta Ct}$ method. Primers for RT-qPCR are listed in Table 2:

Statistical analysis
Statistical analysis was conducted in SPSS Statistics 20. Our data met a normal distribution. Therefore, they were analyzed using an unpaired t-test. P-value < 0.05 was considered significant.

Results
Differential genes identification
Limma is a differential expression screening method based on generalized linear models, and we used the R package limma (version 3.40.6) from the GEO data set (GSE93272), setting |logFC |>1.2 and $p < 0.05$, identifying a total of 1608 DEGs including 1329 up-regulated and 279 down-regulated genes (**Supplementary Table 1**). Volcano plots of DEGs are shown in Fig. 2A. Figure 2B shows the heat map of the first 20 DEGs.

Differential genes functional enrichment analysis
GO and KEGG enrichment analysis of the 1,608 DEGs were performed using the R software package clusterProfiler (version 3.14.3). Set P-value < 0.05. The bubble plot was then used to show the top 10 DEGs GO categories (Fig. 3A-C). The top 10 enrichment terms in KEGG(Fig. 3D). BP enrichment in the cell activation, immune system process, immune system development, regulation of body fluid levels, immune system process, cellular response to stress, positive regulation of immune system process, actin cytoskeleton organization, lymphocyte activation, regulation of T cell receptor signaling pathway(Fig. 3A). CC was mainly enriched in the cell-substrate adherens junction, nucleoplasm part, nuclear part, nuclear lumen, actin filament, cytoskeleton, immunological synapse, actin cytoskeleton, actomyosin, interleukin-6 receptor complex (Fig. 3B). MF was enriched in the cytokine binding, cytokine receptor activity, signaling receptor binding, G protein-coupled chemoattractant receptor activity, C-C chemokine receptor activity, ATPase activity coupled, cytoskeletal protein binding, phosphatase binding, interleukin-17 receptor activity, CD8 receptor binding(Fig. 3C). Moreover, KEGG

Number	Gene name	Primer sequence (5′ to 3′)	Species
1	OXSM-F	TGATGCTGGTCACATAACTGC	*Homo sapiens*
2	OXSM-R	TCCCAATGGTGTGGAAGTAGC	*Homo sapiens*
3	GAPDH-F	GGAGCGAGATCCCTCCAAAAT	*Homo sapiens*
4	GAPDH-R	GGCTGTTGTCATACTTCTCATGG	*Homo sapiens*

Table 2. PCR primer sequence.

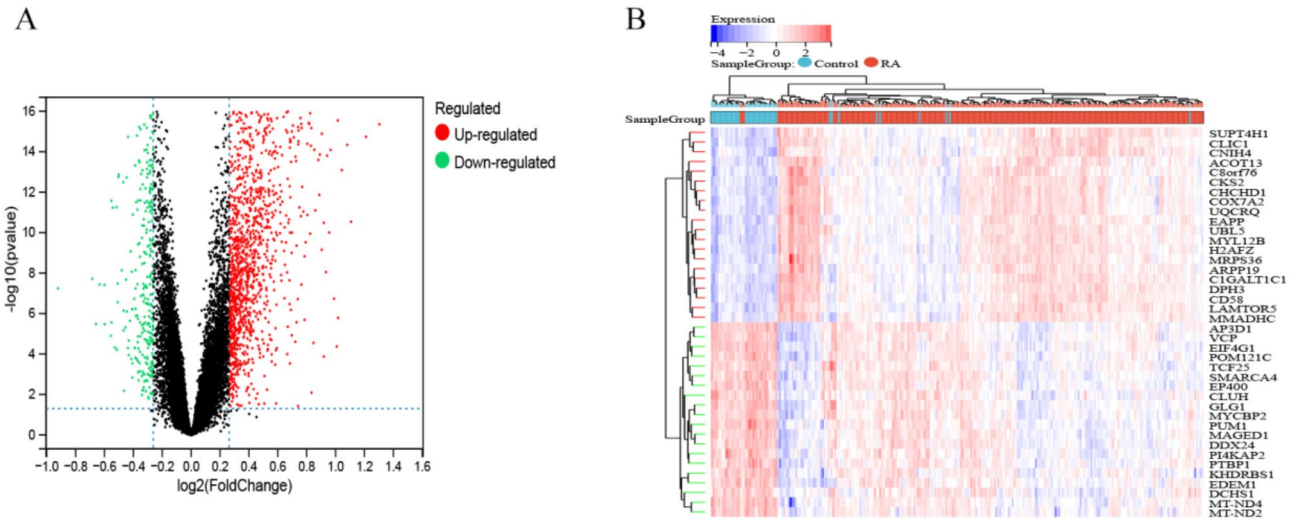

Fig. 2. (**A**) Volcano plot of DEGs (|log2FC| > 1.2 and $p < 0.05$). (**B**) Heatmap of top 20 DEGs.

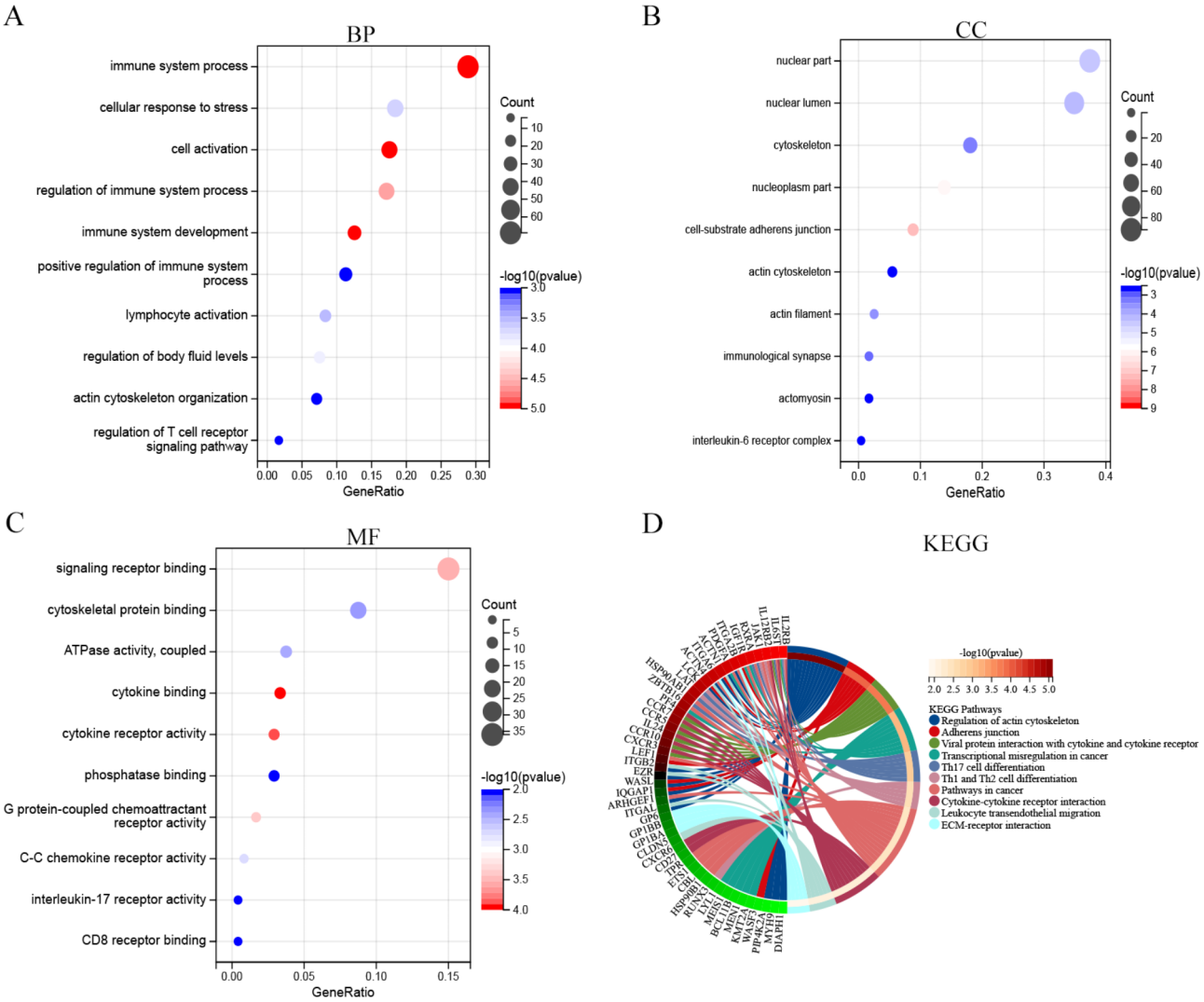

Fig. 3. GO and KEGG enrichment analysis of DEGs. (**A**) BP term analysis. (**B**) CC term analysis. (**C**) MF term analysis. (**D**) KEGG term analysis.

analysis revealed that DEGs are mainly involved in the Regulation of actin cytoskeleton, Adherens junction, Viral protein interaction with cytokine and cytokine receptor, Transcriptional misregulation in cancer, Th17 cell differentiation, Th1 and Th2 cell differentiation, Pathways in cancer, Cytokine-cytokine receptor interaction, Leukocyte transendothelial migration, ECM-receptor interaction(Fig. 3D).

Weighted gene co-expression network analysis

Scale-free co-expression networks were constructed using the sample gene method to remove outliers and samples in the R package WGCNA. Through the Sangerbox platform, the power of $\beta = 12$ (scale-free $R^2 = 0.85$) was automatically set as the soft threshold to produce a scale-free network, ensuring the robustness of the network construction[68–70](Fig. 4A, B). A module merge threshold of 0.25, a sensitivity of 3, and a minimum module size of 30 yielded 16 different co-expression modules (Fig. 4E). Then, the correlation with clinical characteristics (Fig. 4C, D), module membership (MM) and gene significance (GS), and greenyellow module ($r = 0.51$,$p = 2.8e^{-59}$; Fig. 4F) and green module ($r = 0.35$,$p = 1.2e^{-81}$; Fig. 4G) were selected for further analysis.

Feature genes identification and GSEA analysis

1608 DEGs, 934 module genes(**Supplementary Table 2**), and 84 DRGs were crossed to obtain two feature genes, OXSM and ACTN4 (Fig. 5A). We next validated the expression levels of the two feature genes in GSE93272. Violin plot results show that the OXSM gene is highly expressed in RA (Fig. 5B). In contrast, ACTN4 is lowly expressed in RA (Fig. 5C). To understand further the role of feature genes in the pathogenesis of RA, we performed single-gene GSEA analysis. The results showed that OXSM was in the Spliceosome, Peroxisome, Oxidative phosphorylation, and Proteasome, Regulation of the actin cytoskeleton, and Medium enrichment (Fig. 5D). ACTN4 was mainly enriched in the Proteasome, Peroxisome, Regulation of the actin cytoskeleton, Oxidative phosphorylation, and Chemokine signaling pathway (Fig. 5E).

Hub genes identification and diagnostic model construction

We identified hub genes by multivariate Cox regression analysis and receiver operating characteristic (ROC) curves. Using the R package survival, the prognostic value of survival time and two feature genes was evaluated by integrating the survival time data and survival status in 275 samples. As shown in Fig. 6A, OXSM had a significant prognosis compared to ACTN4 ($p = 0.02$). The feature genes were also evaluated for diagnostic value, and the accuracy of the prediction power of the two feature genes was assessed by calculating the Area Under Curve (AUC)value. As shown in Fig. 6B, C, the AUC values of the two feature genes were 0.802 and 0.778, and the hub genes were screened using AUC > 0.800. In summary, OXSM was selected as the hub gene for further validation in this study.

Diagnostic model validation

To verify the expression levels of hub genes and the precision of the diagnostic model, we used GSE45291 external independent datasets for validation. The boxplot results showed that the OXSM genes were highly expressed in RA patients (Fig. 7A), consistent with the results in the training set. The risk score was calculated using coefficient values obtained from multivariate Cox regression analysis through the Sangerbox online platform, and the OXSM gene diagnostic model was validated in the validation set GSE45291. As shown in Fig. 7B, the ROC curve showed an AUC value of 0.982 (95%CI 0.970–0.993), which was higher than the training set, indicating that the model has excellent diagnostic efficiency (Fig. 6B). Notably, GSE45291 is a blood sample dataset[71], showing excellent test results, highlighting the advantage of OXSM as a novel potential biomarker for the diagnosis of RA.

Immune infiltration analysis

The immune microenvironment is essential for clinical treatment sensitivity and disease diagnosis[72]. This study used CIBERSORT to calculate the proportion of 22 immune-infiltrating cells in RA and healthy controls (Fig. 8A, B). The results showed that eight immune cells differ between RA and healthy controls (Fig. 8C). Specifically, Gammadelta T cells and M2 macrophages were highly infiltrated in the RA group, while CD8 + T cells, Regulatory T Cells (Tregs), and Naive CD4 + T cells were significantly reduced. Further, we explored whether OXSM is associated with immune cell infiltration by using the Spearman analysis (Fig. 8D). Correlation analysis showed that OXSM showed a significant positive correlation with Gammadelta T cells, macrophage M2 and a significant negative correlation with Regulatory T Cells (Tregs) and Neutrophils. These lines of evidence suggest that changes in the immune microenvironment in RA patients may be related to OXSM. They also highlight the critical role of OXSM in the immune microenvironment of RA.

Construction TFs-Gene-miRNAs network

The Transcription factors(TFs) and miRNAs for OXSM were predicted using the NetworkAnalyst online tool. Finally, 34 TFs and 8 miRNAs for OXSM were obtained (**Supplementary Tables 3**, **4**). A TFs-gene-miRNAs network(Fig. 9A)containing 43 nodes and 42 edges were constructed using cytoscape, where hsa-mir-7-5p has been linked to the pathological progression of RA[73]. Further, we analyzed the correlation of OXSM with TFs in dataset GSE93272 using spearman. As shown in Fig. 9B, OXSM positively correlated with embryonic ectoderm development(EED)[74], TATA-box binding protein associated factor 7(TAF7) and zinc finger protein 639 (ZNF639) and negatively with non-centrosomal microtubule array protein 1(NOCA1) and cut like homeobox 1(CUX1), suggesting that the above TFs may play a role in the regulation of OXSM expression. We analyzed the TFs-gene-miRNAs interaction network and predicted five significant TFs and eight miRNAs as regulators of OXSM expression.

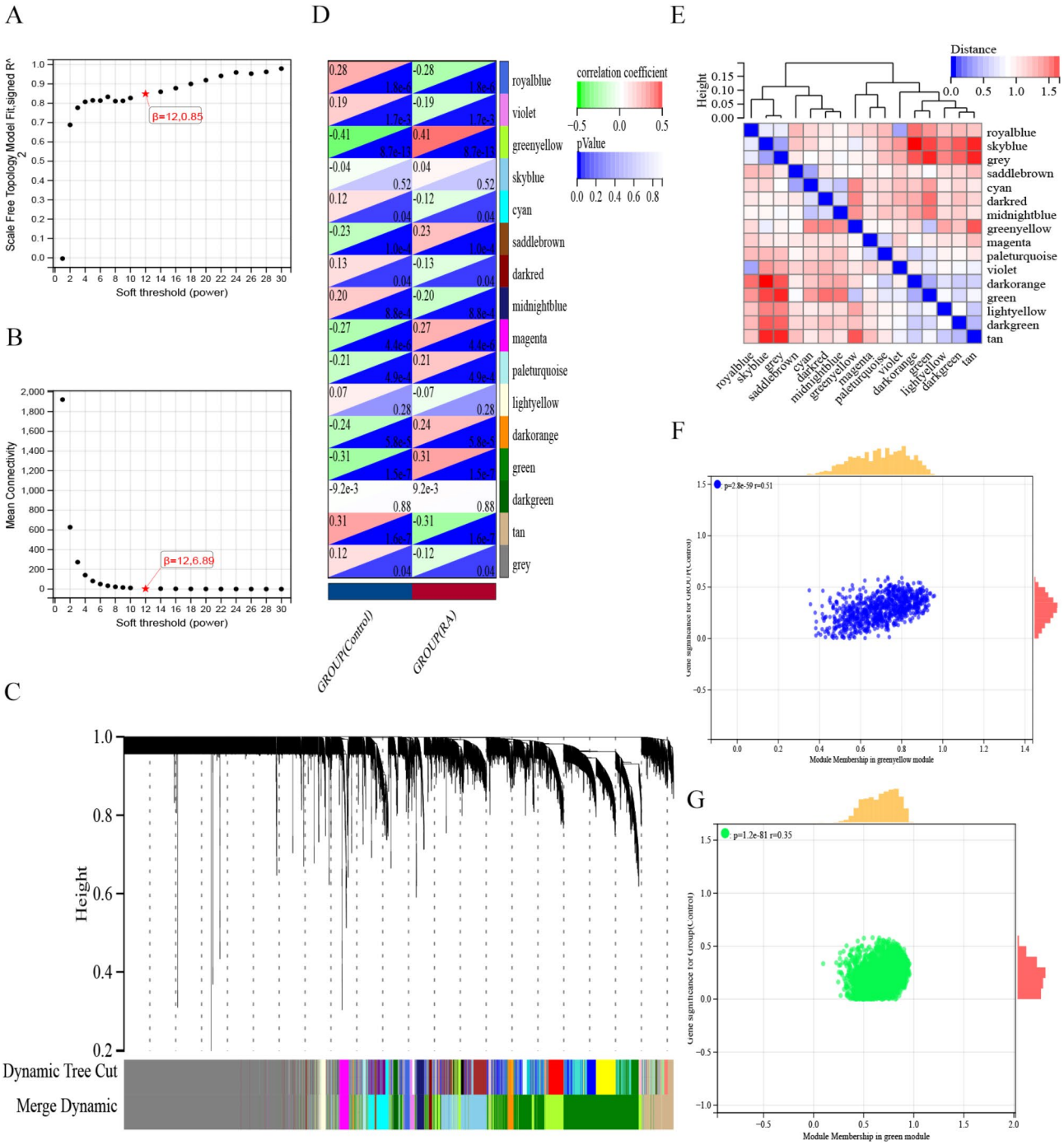

Fig. 4. Results for WGCNA. (**A**) Scale-wise independence of the expression matrix. (**B**) Average connectivity values of the expression matrix. (**C**) Cluster dendrogram of the genes. (**D**) Correlation between the different modules and the clinical characteristics. Red indicates a positive correlation, and green indicates a negative correlation. (**E**) Module vector clustering heatmap. (**F**) Correlation between the module membership degree and the gene significance in the green-yellow module. (**G**) Correlation between the module membership degree and gene significance in the green.

Potential therapeutic drug prediction

Twelve predicted drugs against OXSM were obtained through CTD (**Supplementary Table 5**). Through molecular docking, we selected the top 10 drugs with the lowest binding energy, and the relationship between targets, drugs, and diseases was revealed through the sankey diagram (Fig. 10A). Among the predicted drugs, doxorubicin[75], sunitinib[76], and schizandra B[77] have been documented or studied as targeted drugs for RA, demonstrating the high confidence in drug candidates for RA.

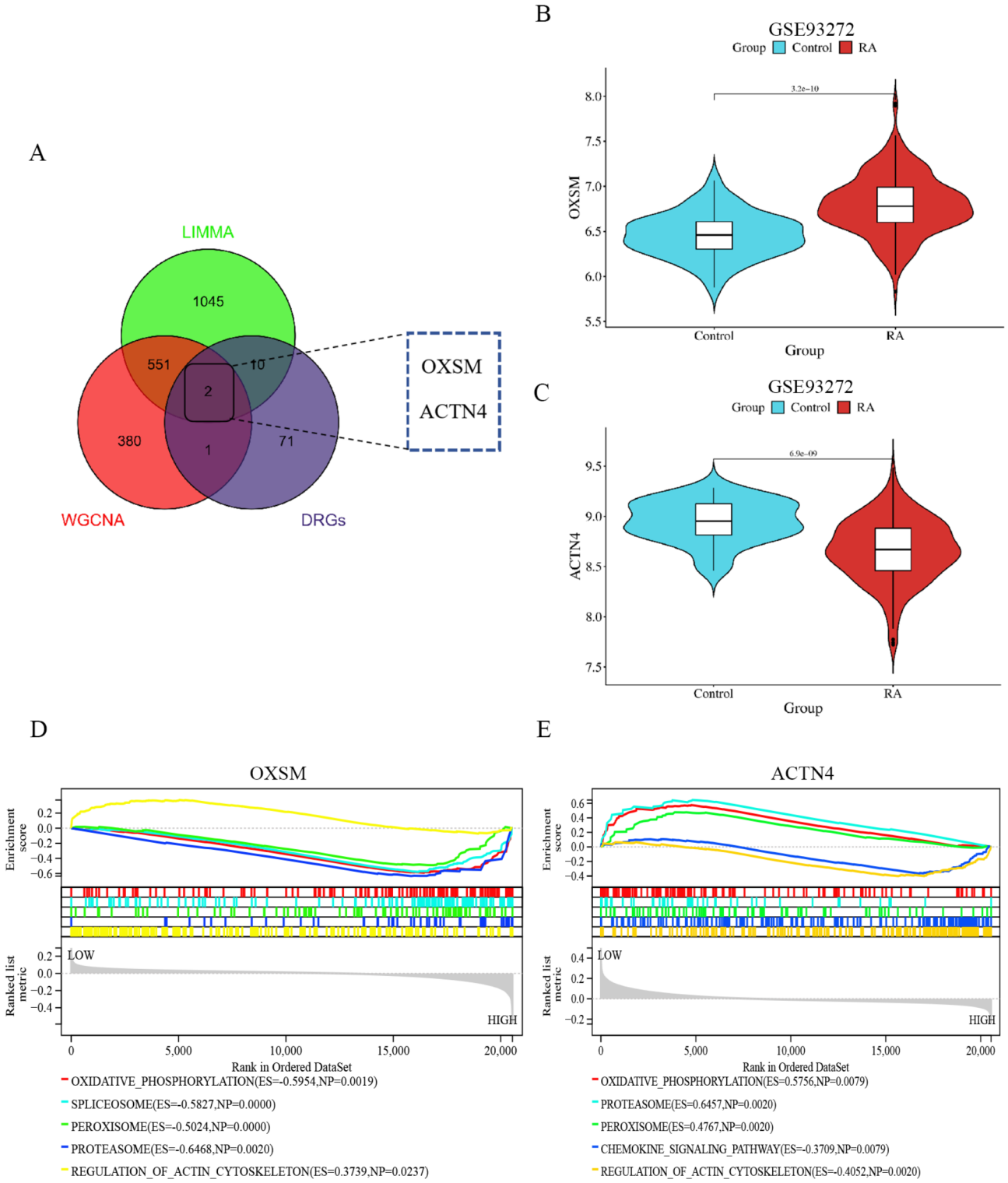

Fig. 5. Feature genes identification and GSEA analysis. (**A**) Venn diagram of LIMMA, WGCNA, and DRGs. (**B**) OXSM gene expression levels in the GSE93272 experiment set. (**C**) Expression levels of the ACTN 4 genes in the GSE93272 experiment set. (**D**) GSEA analysis of the OXSM gene. (**E**) A GSEA analysis of the ACTN4 gene.

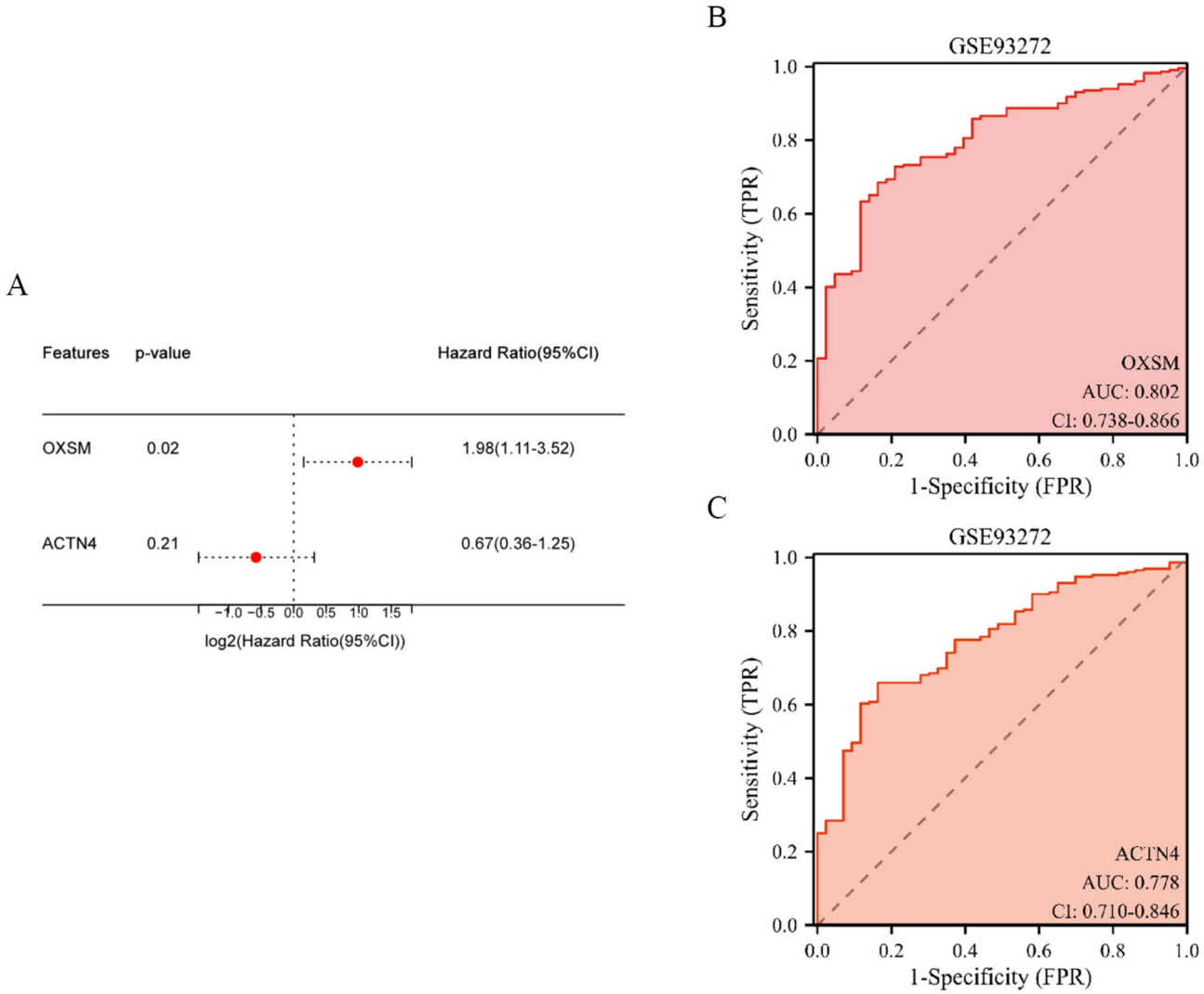

Fig. 6. Multivariate Cox regression analysis and diagnostic value of the feature genes in training set GSE93272. (**A**) Multivariate Cox results for two feature genes. (**B**) ROC curve of the diagnostic model of OXSM in the GSE93272 training set. (**C**) ROC curve of the diagnostic model of ACTN4 in the GSE93272 training set.

Molecular docking validation

Molecular docking is used to assess the binding capacity of the ligand and the receptor, and the smaller the binding energy, the tighter the ligand binds to the protein. A binding energy of less than − 4.25 kcal/mol indicates a specific binding capacity, less than − 5.0 kcal/mol indicates a good binding activity, and less than − 7.0 kcal/mol indicates a solid binding activity[78]. OXSM core proteins were docked to the corresponding 12 predicted drugs using the CB-Dock2 online tool, and all docking binding energy was − 6.0 kcal/mol (**Supplementary Table 6**). The top three were ICG 001 (-10.1 kcal/mol), sunitinib (-8.7 kcal/mol), and doxorubicin (-8.4 kcal/mol), indicating binding solid activity between drug and target protein, especially OXSM and ICG 001. As shown in Fig. 11A, ICG 001 can form hydrogen bonds with ARG252 (length = 2.2 Å) THR315 (length = 3.1Å), which greatly increases the stability of the complex. To compare the stability of ICG 001 and known rheumatoid drug binding to the target, six FDA-approved drugs of Auranofin, Ibuprofen, Leflunomide, MethylprednisoloneTablets, Nimesulide, and Methotrexate for rheumatoid RA were selected with OXSM for molecular docking analysis. The binding energy of these drugs with OXSM is -6.1 kcal/mol, -6.7 kcal/mol, -8.0 kcal/mol, -8.5 kcal/mol, -8.5 kcal/mol, -9.3 kcal/mol, respectively (**Supplementary 7**). Finally, the docking results were visualized using pymol software (Fig. 11A-C).

Molecular dynamics simulations validation

Affinity values indicate the stability of the bond between the receptor and the ligand, with lower affinity indicating that the bond is more stable[79]. Considering that OXSM has the lowest binding energy to ICG 001, we chose the OXSM-ICG 001 complexes for molecular dynamics simulations. These simulations help to analyze the dynamic interactions within the protein-ligand complexes and to validate the molecular docking results[80]. Root mean square deviation (RMSD) is used to observe the overall protein conformational changes of the system

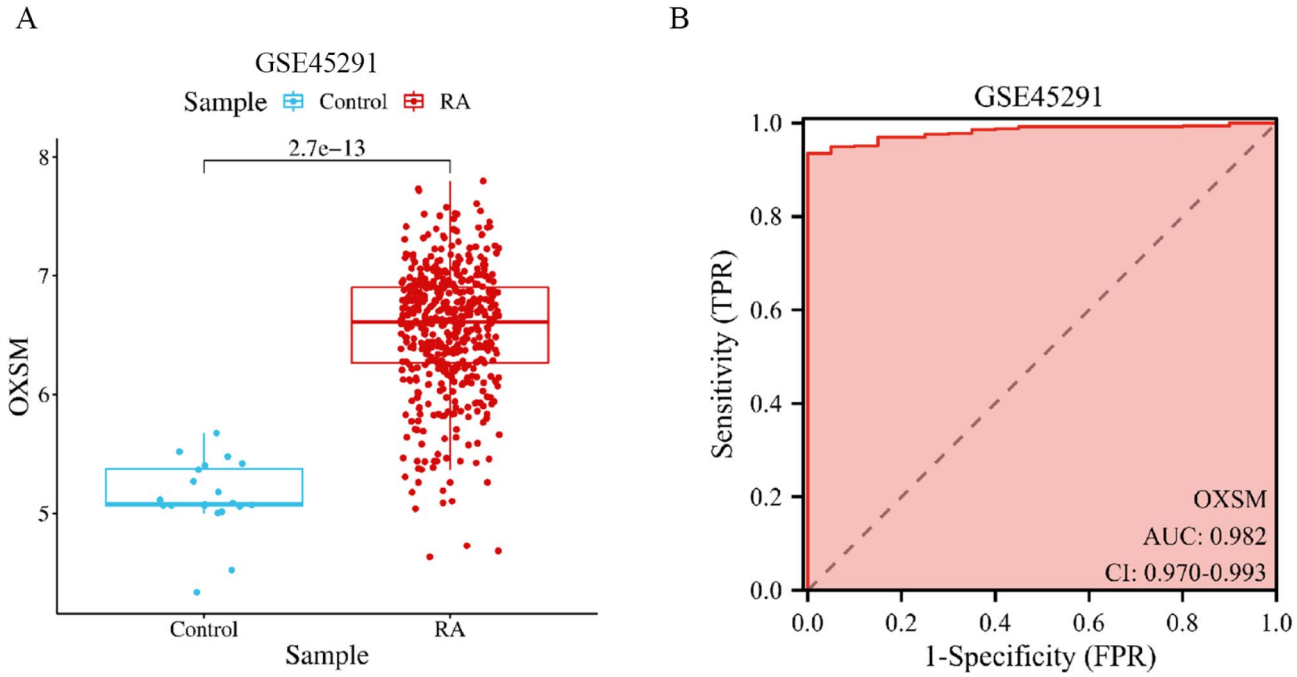

Fig. 7. The expression patterns and diagnostic performance validation of OXSM in the GSE45291 dataset. (**A**) The expression pattern of OXSM in the GSE45291 dataset. (**B**) Diagnostic efficacy of OXSM in the GSE45291 dataset.

relative to the initial structure during the simulation. The larger values indicate a more significant structural change of the protein in the system. As shown in Fig. 12A, the system protein and small molecule RMSD have some fluctuations in the early kinetic period (0-10ns), and at 10-100ns, the RMSD remains around 0.18 nm and 0.40 nm, respectively, indicating the stability of the interaction between ICG 001 and OXSM. Root Mean Square Fluctuation (RMSF) reflects the fluctuation of the site structure of amino acid residues during the simulation, and the larger the value is, the more flexible the residue at this position is. As shown in Fig. 12B, the RMSF of all residues is less than 0.20 nm, with slight overall fluctuation and relatively stable.

The Radius of gyration (Rg) is used to evaluate the tightness of the architecture. The smaller values indicate a tighter protein. It can be found from Fig. 13A that the protein system is within 0-100ns, with a little tight degree, and stable at about 2.60 nm, which is relatively balanced overall. Solvent-accessible surface area (SASA) is the area of the protein surface accessible by the solvent, which measures the area of the protein surface in contact with the solvent. According to the atomic charge range from − 0.20 to 0.20 as the hydrophobic region and the other area as the hydrophilic region, the area of the two parts is counted. As shown in Fig. 13B, the solvent-accessible surface area of the whole system is relatively stable.

Further, we also analyzed the hydrogen bonds formed between proteins and ligands, as shown in Fig. 14A, a 100ns molecular dynamics simulation of the protein-ligand hydrogen bond interaction, and the number of hydrogen bonds formed between 1 and 3 that contributed to the binding. As shown in Fig. 14B, after 100ns of simulation, the ligand remained tightly bound in the protein cavity.

The binding free energy of protein and small molecules changes with time, and the lower the binding free energy, the stronger the binding force[81]. As shown in Fig. 15A, the binding free energy contribution of small molecules and protein mainly comes from ARG-252, LEU-354, ASP-272, and ALA-253 of protein A chain. The binding free energy − 41.23 kcal/mol (Fig. 15B) was calculated by MM/GBSA, and the lower the binding energy, the stronger the binding capacity. Free energy landscape (FEL) characterizes the change in the free energy of matter experienced during the simulation. Calculating the free energy topography of the protein and ligand complexes can guide the characteristic conformations of the extracted complexes. Meanwhile, the protein's free energy topography shows the protein conformation's stability. Figure 15C shows the free energy topography of the protein, which dominates the complexes conformation ranging from 0.10 to 0.14 nm and RMSD from 2.525 to 2.540 nm.

Ramachandran plot is a visualization method developed by G. N. Ramachandran et al. in 1963 in the protein structure[82]. It can also reflect whether the conformation of the protein is reasonable. Ramachandran Plot displays the structural features of the protein backbone by drawing the dihedral angles (φ and ψ angles). The scatter concentration region contains reasonable regions of dihedral angles. These regions represent stable conformations in the protein structure. Generally, reasonable dihedral angle regions include the α helical region, β folding region disordered region, etc. Regions where scatter does not exist are the abnormal or forbidden dihedral angles. These regions represent conformations with little or no appearance in the standard protein structure.

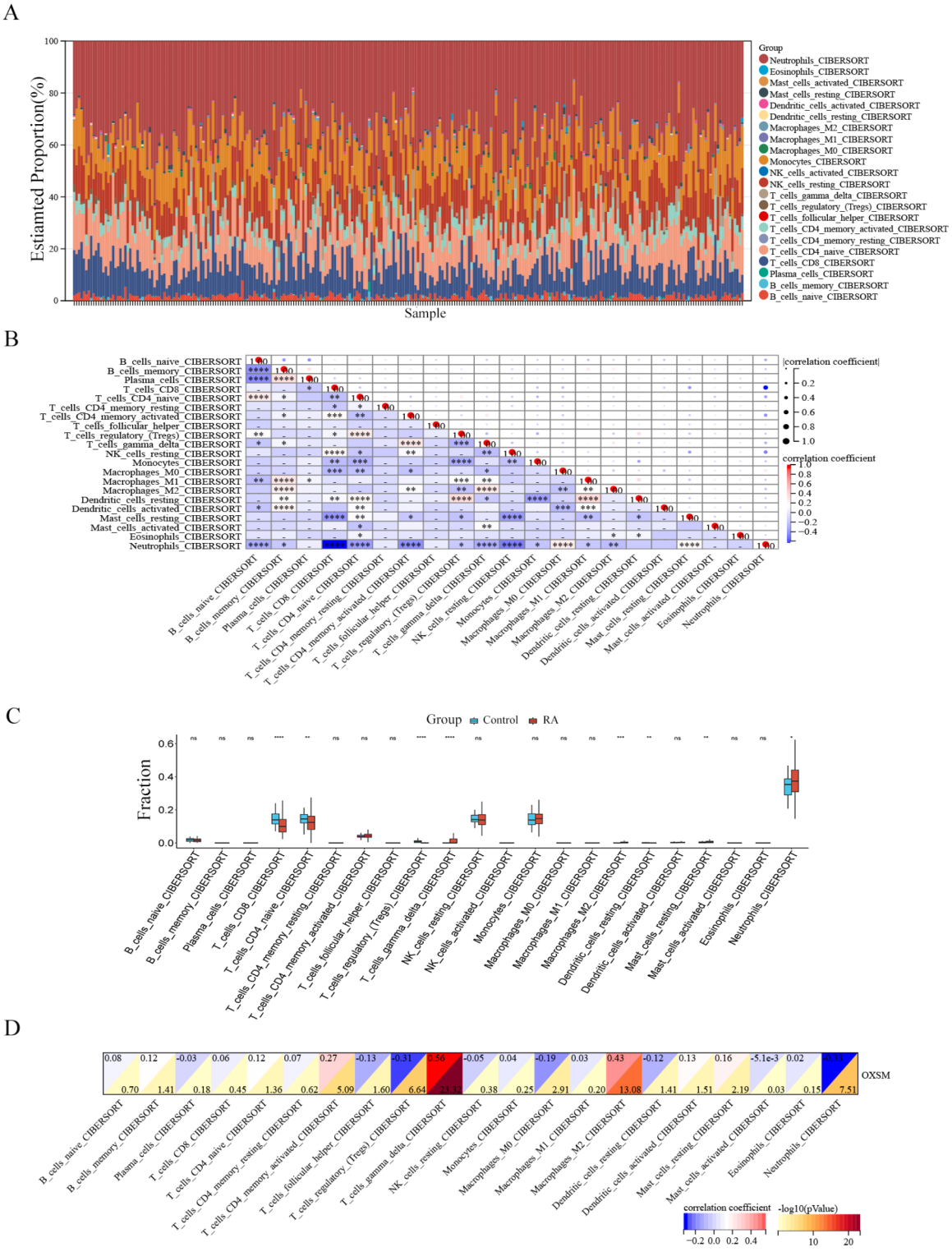

Fig. 8. Analysis of immune cell infiltration between RA and healthy control. (**A**) Relative abundance of the 22 infiltrating immune cells between the RA and healthy control groups. (**B**) Heatmap of the correlation between 22 immune cells. (**C**) Boxplots showing the difference in immune-infiltrating cells between the RA and healthy control. $*p<0.05$, $**p<0.01$, $***p<0.001$. (**D**) Correlation between the OXSM and immune-infiltrating cells.

Figure 16A, B is the standard Ramachandran Plot, Fig. 16C is the overall diagram of complexes proteins, Fig. 16D is the glycine, Fig. 16E is the dihedral angle distribution of the previous residue of proline, and Fig. 16F is the dihedral angle distribution of proline. The unique structural properties of glycine and proline affect the distribution of their dihedral angles (φ and ψ), thus affecting the folding and function of the entire

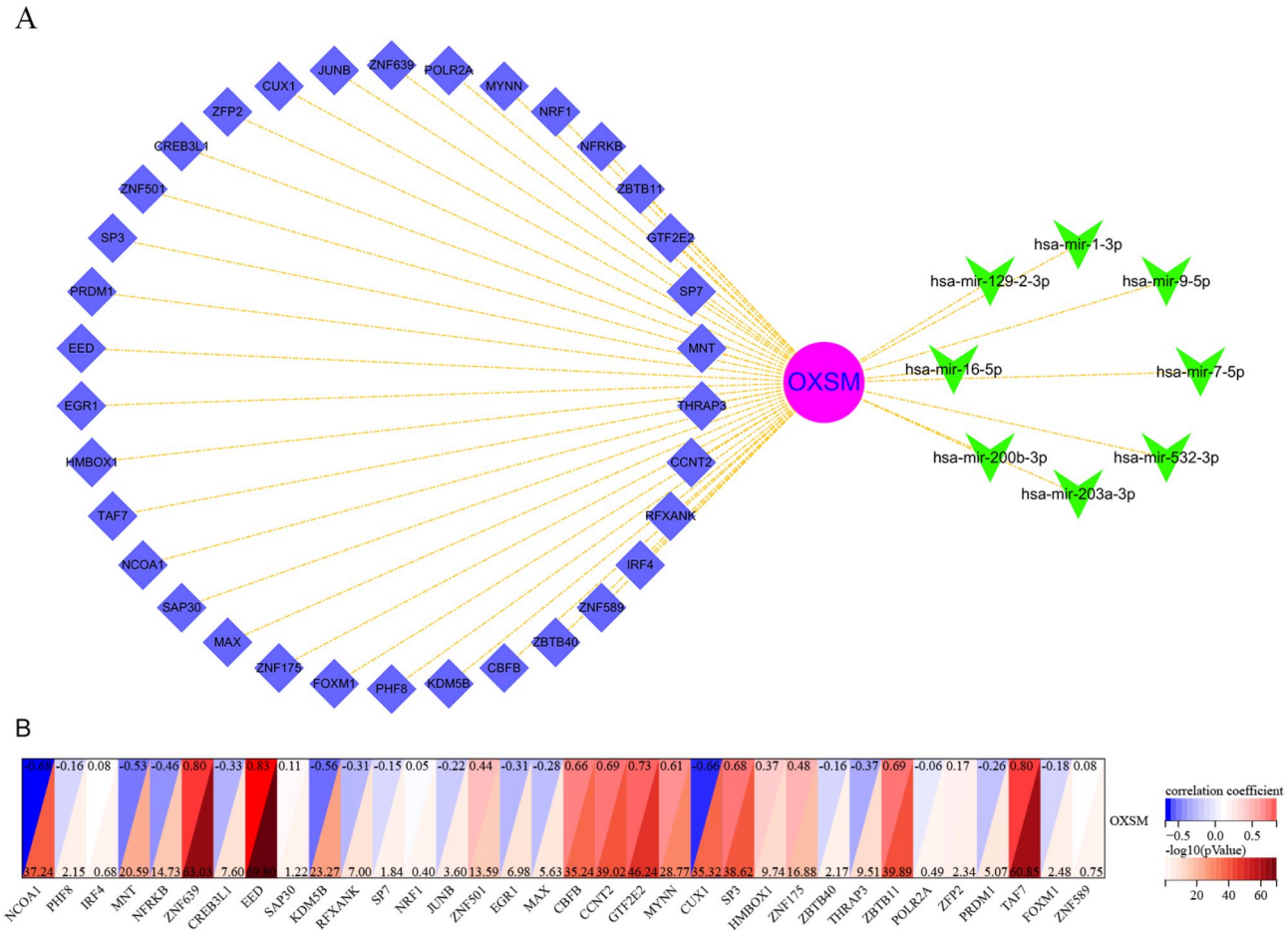

Fig. 9. The TFs-gene-miRNAs network construction. (**A**) The TFs-gene-miRNAs network based on the hub gene.The purple balls represent hub gene, green triangles represent miRNAs and blue diamonds represent TFs. (**B**) Heatmap of the correlation between OXSM and TFs in GSE93272.

protein. Compared with the standard Ramachandran Plot (Fig. 16A, B), most scattered points are distributed in reasonable areas, and only a few parts are scattered in other regions. Overall, the OXSM proteins bound to ICG 001 showed a spatially acceptable molecular conformation after the MD simulation, indicating the stability of the complexes.

RT-qPCR validation hub gene expression

RT-qPCR verified the expression level of the hub genes and showed significantly higher OXSM expression in peripheral of RA compared to healthy controls (Fig. 17A).

Discussion

Rheumatoid arthritis, an autoimmune disease with multiple etiology, has been extensively studied and has made some progress[83,84]. However, due to the lack of sufficient specific biomarkers and the heterogeneity of RA pathogenesis, the early diagnosis and treatment of RA still face challenges[85–87]. Therefore, searching for newer and more effective diagnostic markers and therapeutic targets is crucial for the early diagnosis and individualized treatment of RA[51]. Disulfidptosis is a newly discovered form of cell death due to the accumulation of disulfide, ultimately leading to cell death[19]. Studies have shown that disulfidptosis-related genes can regulate the secretion of pro-inflammatory cytokines, leading to the development of autoimmune diseases such as psoriatic arthropathy (PsA), ankylosing spondylitis (AS), juvenile idiopathic arthritis (JIA) and rheumatoid arthritis (RA)[34,88]. It was shown that disulfide stress-mediated disulfidptosis is involved in the immature differentiation of upper basement cells in psoriasis[89]. Although disulfidptosis has been studied in several inflammatory diseases[90], the specific mechanism, regulatory role and potential targets in RA have not been elaborated.

Our study aimed to identify and validate novel biomarkers associated with disulfidptosis in RA and to reveal the underlying mechanisms. We downloaded the GSE93272 dataset from the GEO database as a training set and identified 1329 upregulated DEG and 279 downregulated DEG by extracting gene expression profiles. According to GO functional enrichment analysis, RA-related DEG in BP was mainly enriched in the immune system process, cellular response to stress, cellular response to stress, and T cell receptor signaling pathway regulation. CC was enriched in the nuclear part, actin cytoskeleton, immunological synapse, and interleukin-6

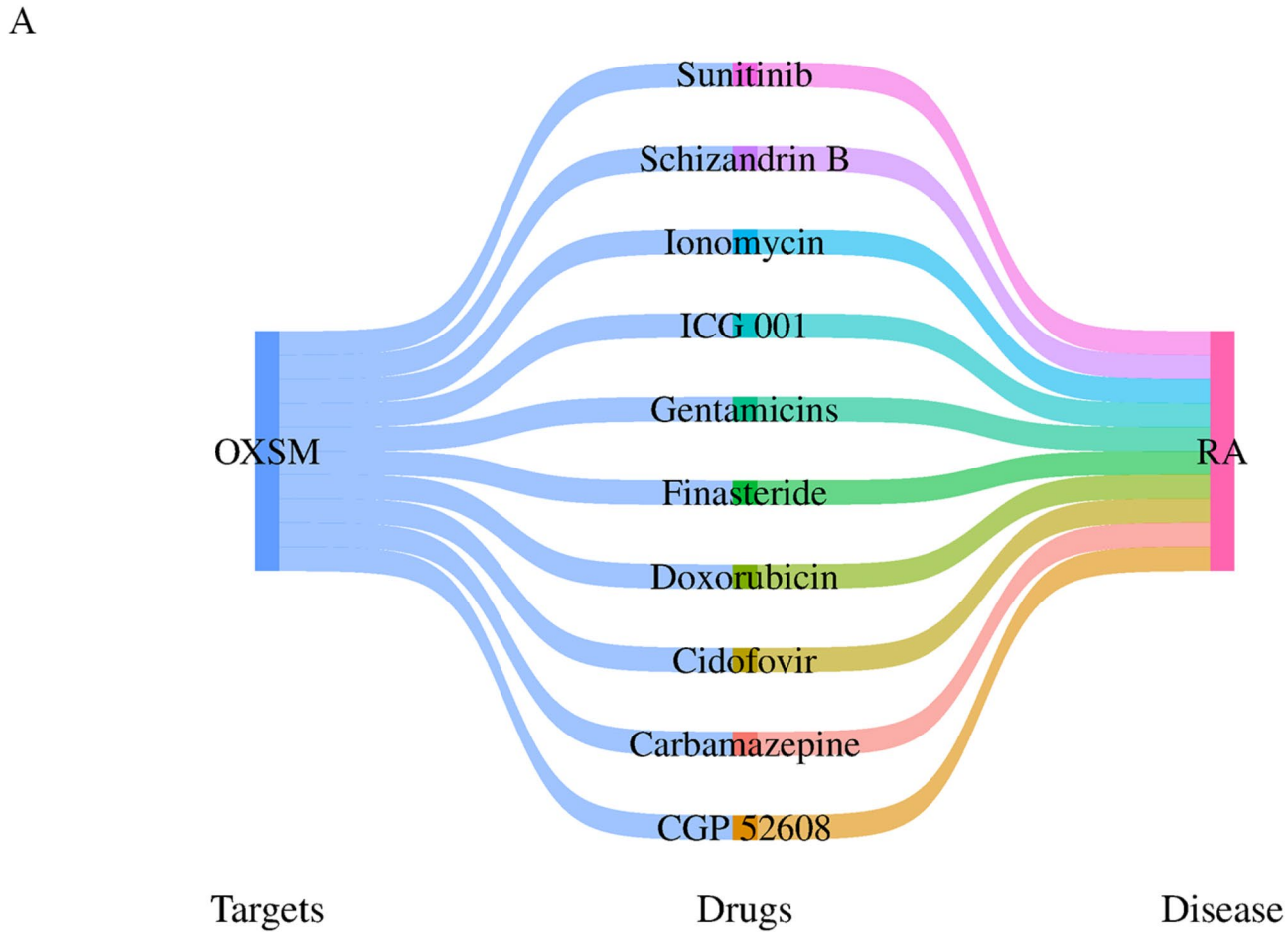

Fig. 10. Prediction of hub gene-targeted drugs. (**A**) The Sankey plot demonstrates the interaction relationship between targets-drugs-disease.

receptor complex. MF was enriched in cytokine receptor activity, cytoskeletal protein binding, interleukin-17 receptor activity, and CD8 receptor binding. KEGG analysis showed that DEGs are enriched in the Regulation of actin cytoskeleton, Viral protein interaction with cytokine and cytokine receptor, Th17 cell differentiation, Th1 and Th2 cell differentiation. These functional enrichment analyses indicate that DEG is enriched in immune response, inflammation, and actin cytoskeleton and plays an important role in the pathogenesis of RA[19,23,24,91].

It has been found that cytoskeletal protein levels are reduced in skeletal muscle of RA patients[23,24,92], suggesting that the deterioration of RA is associated with actin destruction. The actin cytoskeleton plays an essential role in maintaining chondrocyte homeostasis and survival. The collapse of the actin cytoskeleton and the loss of chondrocyte homeostasis lead to the destruction of the cartilage matrix, leading to irreversible chondrocyte damage and ultimately inducing joint inflammation[21,23,24]. Studies have shown that synovial fluid and plasma levels of thiols are reduced, and disulfide levels are significantly elevated in RA, thereby triggering oxidative stress, leading to joint damage, and ultimately inducing RA[23,25–27]. However, during disulfidptosis, the intake of abundant cystine may increase the intracellular concentrations of glutathione and NADPH, thereby reducing reactive oxygen species (ROS) levels. Thus, reducing ROS levels plays a crucial role in the anti-inflammatory pathway and is critical for alleviating and inhibiting RA progression[23,24,85,92]. In this study, we linked disulfidptosis to the pathogenesis of RA, integrated bioinformatics, molecular docking, molecular dynamics simulation, and experimental verification to find the potential essential genes of disulfidptosis in RA, explore the potential therapeutic targets and drugs, and provide new targets and strategies for the future treatment of RA.

We identified two feature genes associated with disulfidptosis from the GSE93272 dataset OXSM and ACTN4. GSEA enrichment showed significant enrichment of feature genes in the peroxisome, oxidative phosphorylation, proteasome, and regulation of the actin cytoskeleton. In order to find markers with higher diagnostic value in clinical diagnosis and treatment, we identified hub genes by multivariate cox regression analysis and receiver operating characteristic curve (ROC) analysis. The results of multivariate survival analysis showed that OXSM had high prognostic significance ($p = 0.02$), and the AUC value corresponding to ROC was 0.802(95%CI:0.738–0.866), 0.778(95%CI:0.710–0.846). The AUC > 0.800 was used as the screening criterion, and finally, OXSM was selected as the hub gene. Further, we validated the expression level of OXSM and the model's accuracy in Dataset

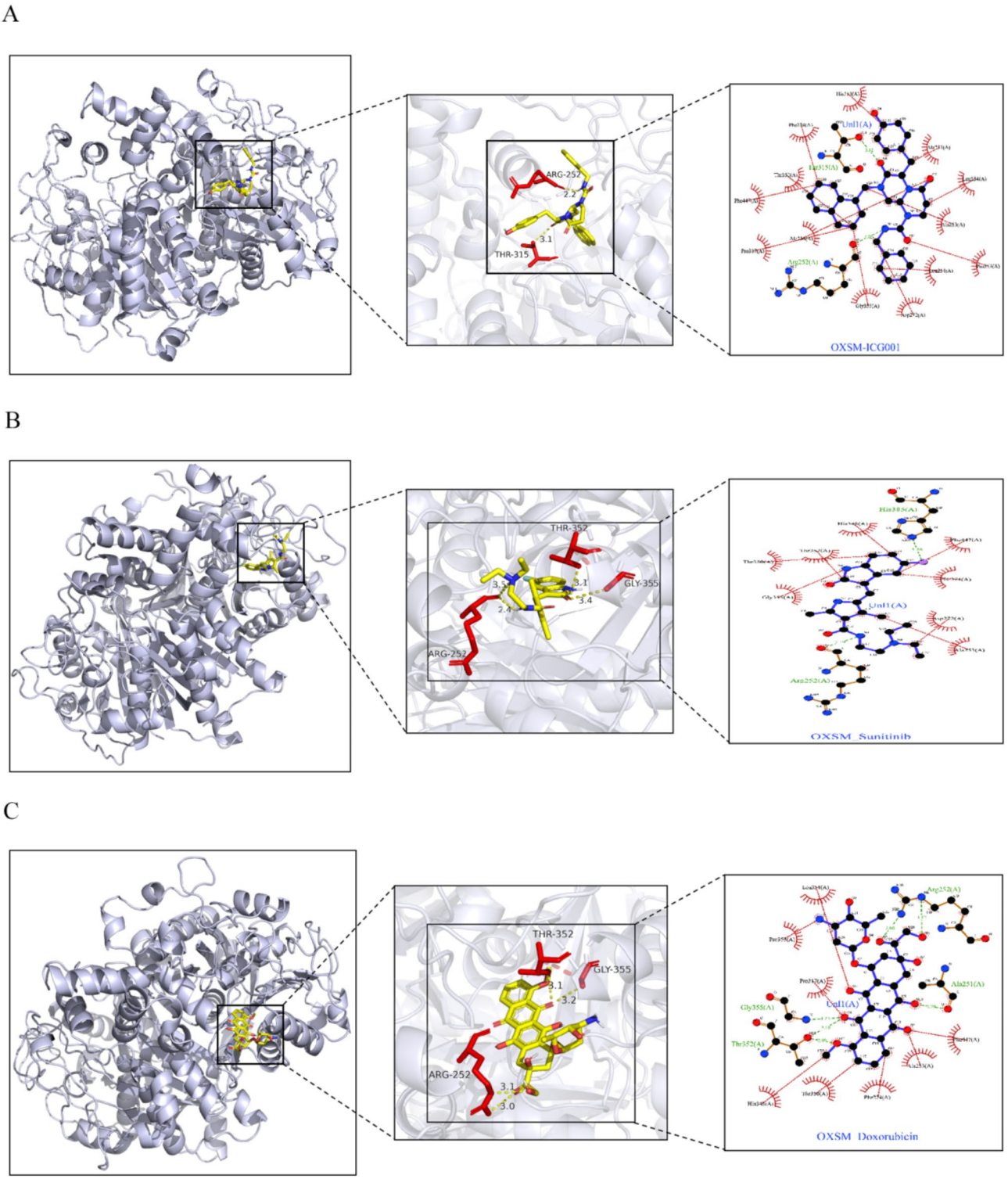

Fig. 11. Diagram of the top three drug binding modes with the lowest molecular docking binding energy to the OXSM protein (PDB id: 2IWZ). (**A**) ICG 001 with OXSM ((− 10.1 kcal/mol). (**B**) Sunitinib with OXSM (− 8.7 kcal/mol). (**C**) Doxorubicin with OXSM (− 8.4 kcal/mol).

GSE45291. The results showed that OXSM was significantly upregulated in the peripheral blood of RA patients with an AUC of 0.982(95%CI:0.970–0.993). Therefore, OXSM performed best as a diagnostic marker.

Oxoacyl-ACP Synthase Mitochondrial (OXSM), also known as FASN2D, is a second essential synthase encoded by nuclear DNA involved in the mitochondrial fatty acid synthesis and extension pathway[93–95]. OXSM, as a disulfidptosis-related gene, plays a vital role in the metabolic pathways of tumor cells and mitochondrial dysfunction diseases[96,97]. The finding of a positive correlation between OXSM levels and plasma cell and T

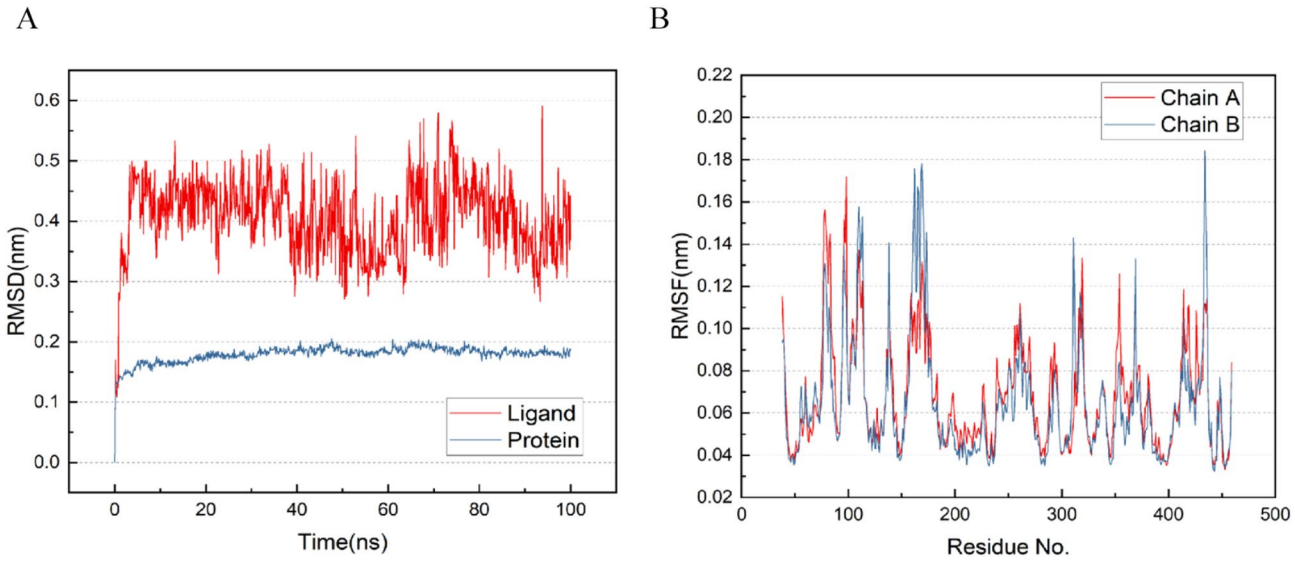

Fig. 12. (**A**) RMSD of the OXSM-ICG 001 complexes under a 100 ns MD simulation. (**B**) RMSF of the OXSM-ICG 001 complexes under a 100 ns MD simulation.

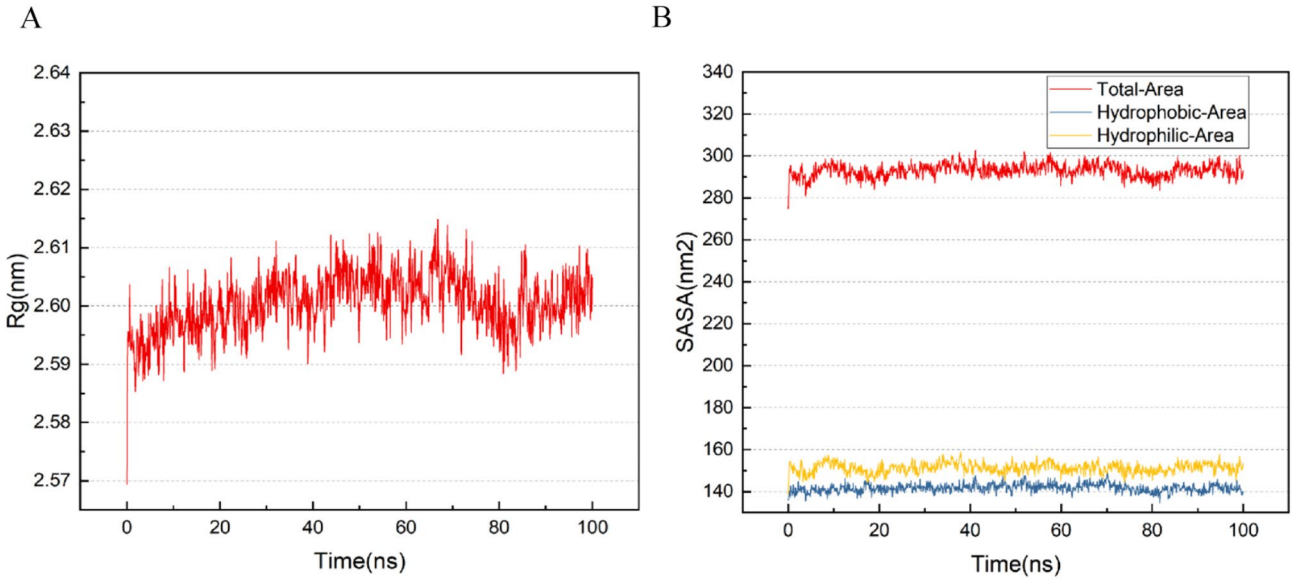

Fig. 13. The radius of gyration (**A**) and solvent-accessible surface area (**B**) of the OXSM-ICG 001 complexes during the 100ns time frame.

cell levels in bladder cancer samples suggests its possible involvement in regulating immune response and inflammation[84]. In metastatic oral squamous cell carcinoma (OSCC), the core binding factor subunit β (CBFB) regulates OXSM expression through cis-specific enhancer-binding of OXSM, controlling the proliferation, invasion, and lipid synthesis of metastatic OSCC cells[95]. In colorectal cancer, CBFB deficiency enhances cellular resistance to MEK, an inhibitor of the targeted mitogen-activated protein kinase (mAPK) pathway[98,99]. Some studies have reported that OXSM can inhibit the growth of ovarian cancer cell lines, disrupt the stability of OXSM by knocking down heat shock protein D family member 1 (HSPD1), and promote the proliferation and migration of ovarian cancer cells[100]Some studies have found that hsa-miR-338-3p participates in fatty acid biosynthesis and metabolism by regulating OXSM levels and is also implicated in the occurrence and proliferation of glioma cells[101].

Studies have shown that mitochondrial dysfunction affects the development of inflammatory diseases by modulating the balance of antigen presentation and immune cells[102]. In RA, mitochondrial dysfunction promotes the occurrence and progression of RA through abnormal energy metabolism, overproduction of reactive oxygen species (ROS), and the activation of innate immunity[96]. Furthermore, mitochondrial dysfunction in

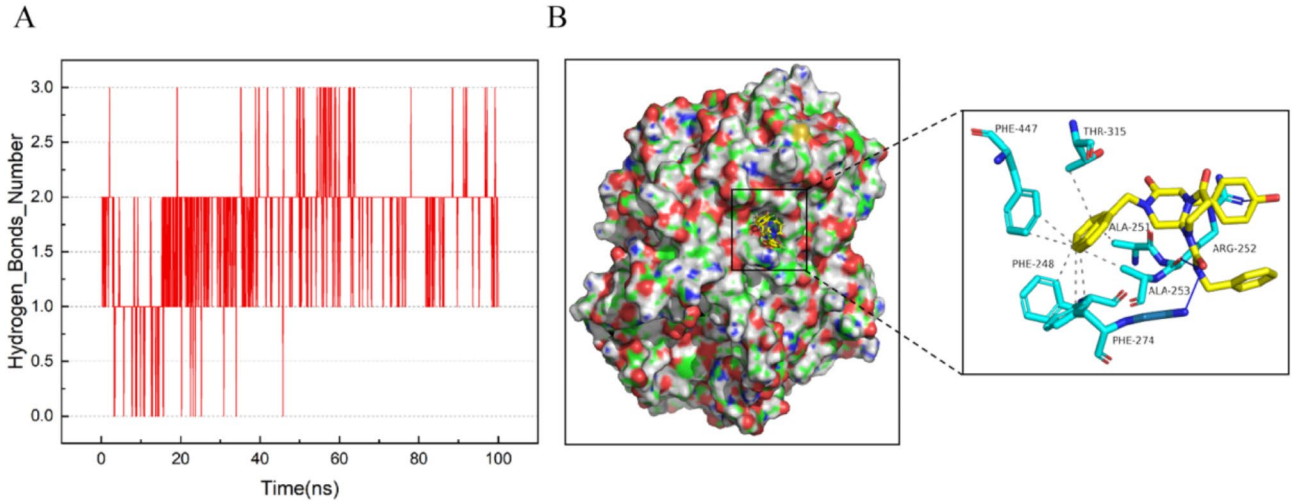

Fig. 14. (**A**) The number of hydrogen bonds in complexes between ICG 001 and OXSM. (**B**) Details of the 3D interaction between ICG 001 and OXSM, yellow stick tick for ICG 001 in the figure and cyan stick tick for amino acids acting with ICG 001. Blue solid lines indicate the hydrogen-bonding interactions.

RA also affects various immune cells, including macrophages, CD4 + T cells, CD8 + T cells, and neutrophils[103]. Disulfidptosis is a phenomenon caused by oxidative stress. Related disulfidptosis genes affect the recruitment and activation of immune cells by regulating the redox state of cells, the release of chemokines, and generating reactive oxygen species (ROS). At the same time, immune cells provide pro-inflammatory or anti-inflammatory signals by changing the immune microenvironment and thus influence the expression of disulfidptosis genes and their function[99].

Furthermore, diabetes and its complications are a disease of mitochondrial dysfunction; the reduction of OXSM increases the risk of nephropathy and atherosclerosis in diabetic patients, and fatty acid deficiency is a risk factor for the onset of diabetic complications[96]. The latest study also found that OXSM plays an essential role in regulating OA's inflammatory response and immune infiltration[85].

Peripheral immune cells are also involved in the pathogenesis of RA[51]. Compared to healthy controlsThe RA group was highly infiltrated with Gammadelta T cells and M2 macrophages, while CD8 + T cells, Regulatory T Cells, and Naive CD4 + T cells were significantly reduced. Correlation analysis showed that OXSM showed a significant positive correlation with gammadelta T cells, macrophage M2 and a significant negative correlation with regulatory T Cells and neutrophils. Studies suggest that gammadelta T cells and M2 macrophages play essential roles in RA's pathogenesis and pathological progression[104,105]. Gamma delta T cells play a unique and important role in autoimmune diseases such as juvenile idiopathic arthritis (JIA), systemic lupus erythematosus (SLE), ankylosing spondylitis (AS), systemic sclerosis (SSc), and rheumatoid arthritis(RA)[106–108]. Studies have found that Gamma delta T cells participate in and activate the inflammatory process in the RA synovium[106]. The increase of gamma delta T cells can promote the production of IL-17 inflammatory factors, thus accelerating the body's inflammatory response[109]. Regulatory T cells (Treg cells) are vital in preserving immune tolerance in peripheral tissues and suppressing autoimmunity and are associated with disease severity[110–112]. Research shows that the imbalance between Treg cells and Th17 plays a crucial role in the occurrence and progression of RA[110]. Studies have found that the number of Treg cells in the peripheral blood of RA patients was reduced[112,113]. Congenital immune cells such as Treg cells can mediate autoimmune responses when the number and/or function of these cells may lead to overproduction of pro-inflammatory cytokines such as IL-1, IL-2, IL-, IL-6, IL-8, and IL-17, accelerate the destruction of articular cartilage, promote synovitis and eventually lead to RA[110,114,115].

Transcription factors (TFs) and miRNA regulate gene expression[116,117]. In GSE93272, we analyzed the correlation of OXSM with TFs and found that EED, TAF7, and ZNF639 were positively correlated with OXSM, indicating that EED, TAF7, and ZNF639 may positively regulate the transcription of OXSM. We also predicted eight miRNAs that interact with OXSM, and some studies found that the altered expression level of hsa-mir-7-5p may be involved in the pathogenesis of RA[73]. The hsa-mir-203a-3p was associated with the occurrence of autoimmune diseases in mice[118]; the hsa-miR-200b-3p was associated with avascular necrosis of the femoral head[119]; the hsa-miR-16-5p was associated with systemic lupus erythematosus and psoriatic arthritis[120,121]; the hsa-miR-1-3p was associated with systemic lupus erythematosus[120], and the hsa-mir-1-3p was associated with SARS-CoV-2 and RA in S. aureus infection[122].

Furthermore, 12 drugs were identified by CTD, which ICG 001, carbamazepine, and sunitinib have potential drugs for the treatment of RA, and molecular docking validation predicted the strength of action between the drug and OXSM. The docking results showed that the binding energy of the 12 drug components to OXSM proteins was all − 6.0 kcal/mol, indicating a strong binding affinity. Notably, the lowest binding energy between ICG 001 and OXSM (-10.1 kcal/mol). Compared with ICG 001, the binding energies of Auranofin, Ibuprofen, Leflunom, Methylprednisolone Tablets, Nimesulide, Methotrexate, and OXSM were − 6.1 kcal/mol, -6. kcal/

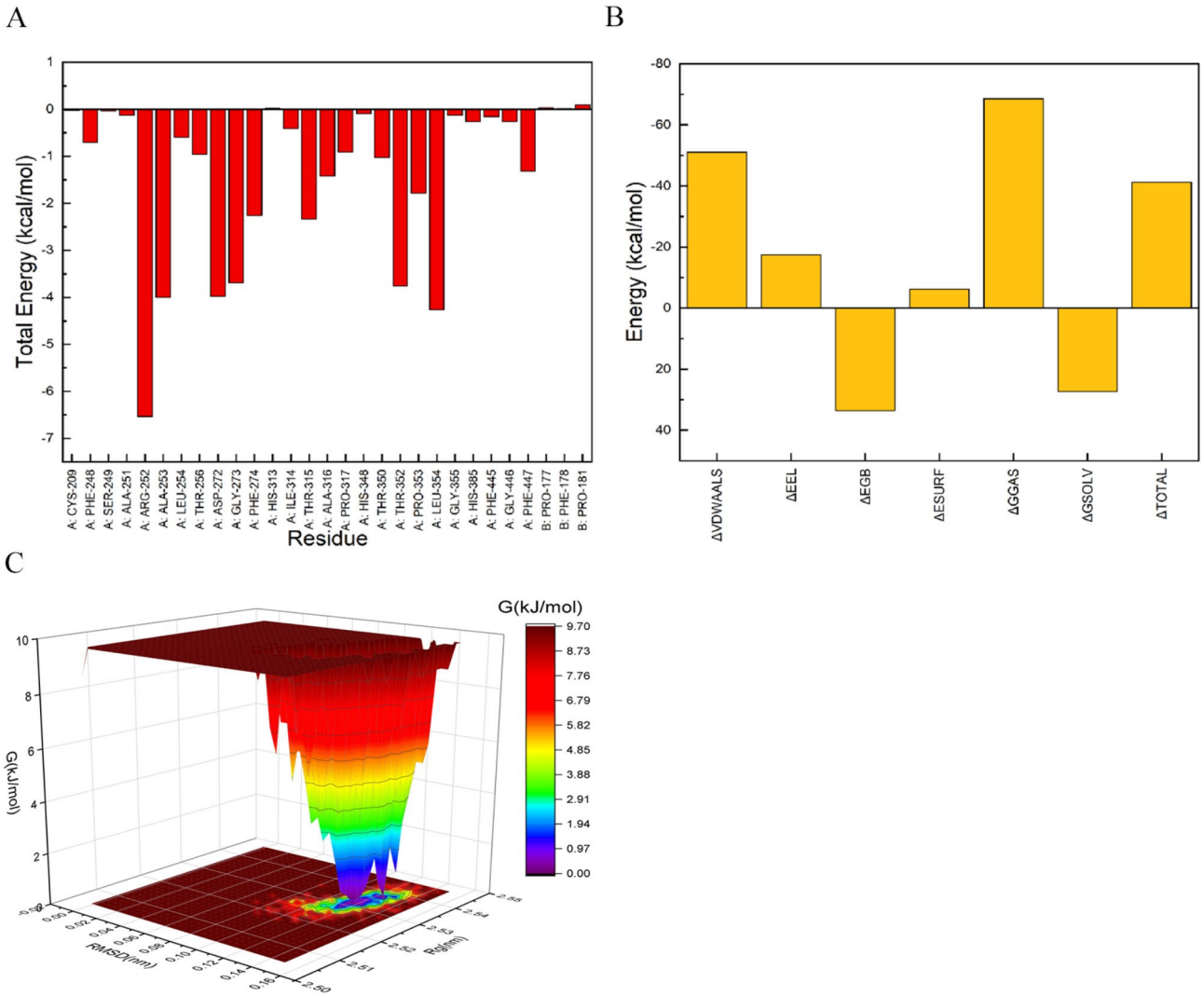

Fig. 15. (**A**) Residues and energetic analysis that contribute substantially to the ICG 001 binding energy. (**B**) The contribution of various interactions to the MM/GBSA score of ligands. (**C**) The free-energy landscape map of the ICG 001-OXSM complexes.

mol, -8.0 kcal/mol, -8.5 kcal/mol, -8.5 kcal/mol, -9.3 kcal/mol, respectively. The results showed that ICG 001 had better binding affinity with OXSM than the six drugs, highlighting its potential as a therapeutic drug. However, we have to admit that molecular docking has limitations. Specifically, our docking simulations used rigid receptor models, which may not be able to explain the dynamic nature of protein conformations. In addition, we note that the scoring functions used in the docking process may not fully capture the complexity of the ligand-receptor, which could lead to differences in the predicted binding affinities. ICG 001 is a transcriptional antagonist[123], and a small molecule inhibitor of the Wnt/β-catenin signaling pathway, which can effectively inhibit the proliferation and migration of a variety of cancer cells[124], reduce the chemotherapy resistance of gastric cancer stem cells[125], induce autophagy of endometrial cancer cells[126], by increasing radiation-induced DNA damage and improve the tumor immune microenvironment to enhance radiotherapy effect[127]and can improve chronic lung injury and prevent progression to severe lung fibrosis[123]. Studies have shown that there is a high level of β-catenin in FLS of RA patients, and a high level of β-catenin can maintain the stable activation of FLS, thus causing the overexpression of inflammatory factors such as TNF-α and IL, which mediate the inflammatory response of RA[128]. The overactivation of the Wnt signaling pathway and abnormal expression of β-catenin play a significant role in RA bone destruction, causing severe disruption to the balance between osteoblasts and osteoclasts required for normal bone remodeling, leading to progressive bone destruction. Therefore, inhibition of the Wnt/β-catenin signaling pathway can help alleviate the occurrence and development of arthritis[129]. Molecular dynamics simulations showed that ICG 001 stably binds to OXSM with a binding free energy of -41.23 kcal/mol, indicating that OXSM is the target of ICG 001. We hypothesized that under glucose starvation conditions, OXSM is aberrantly expressed in RA, triggering disulfidptosis, and ICG 001 may destroy the course of RA by inhibiting OXSM overexpression. Thus, OXSM may be an essential target for disulfidptosis-related mechanisms in RA. However, there are no studies of ICG-001 in treating rheumatoid arthritis. Since side effects of ICG-001

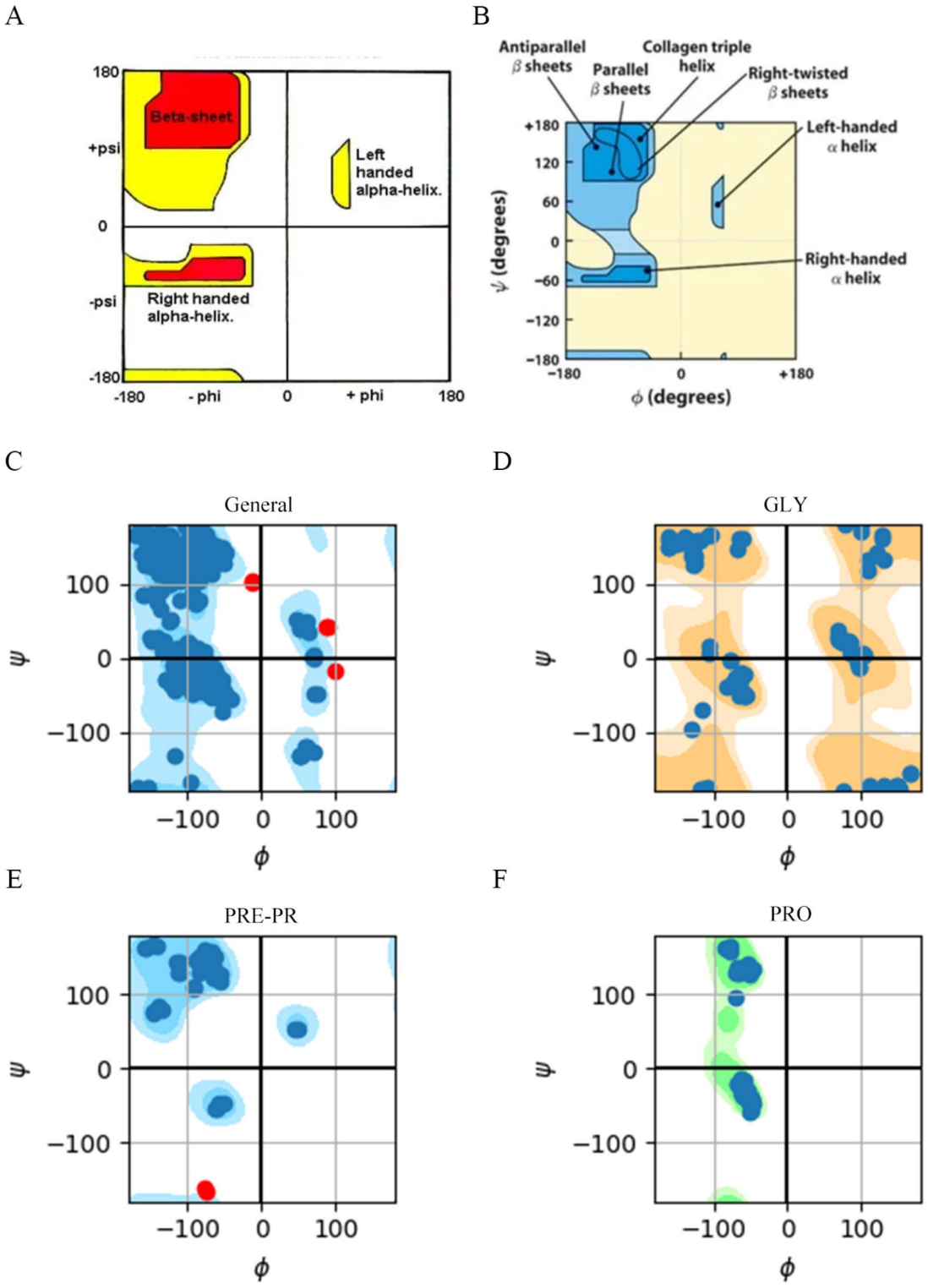

Fig. 16. (**A**) and (**B**) is a standard Ramachandran plot. (**C**) complexes Protein Overall Ramachandran plot. (**D**) Ramachandran plot of glycine. (**E**) Ramachandran plot of the dihedral angle distribution of one residue preceding the proline. (**F**) Ramachandran plot of the dihedral angle distribution of proline.

treatment cannot be entirely excluded, further studies are needed to determine whether the identified OXSM gene is indeed a direct target of ICG-001[130]. Meanwhile, in vivo and in vitro experiments are needed to verify the targeted effect between ICG-001 and OXSM, and chemical modification or nanocarriers may be helpful for reducing the off-target effect of ICG-001 and OXSM.

A

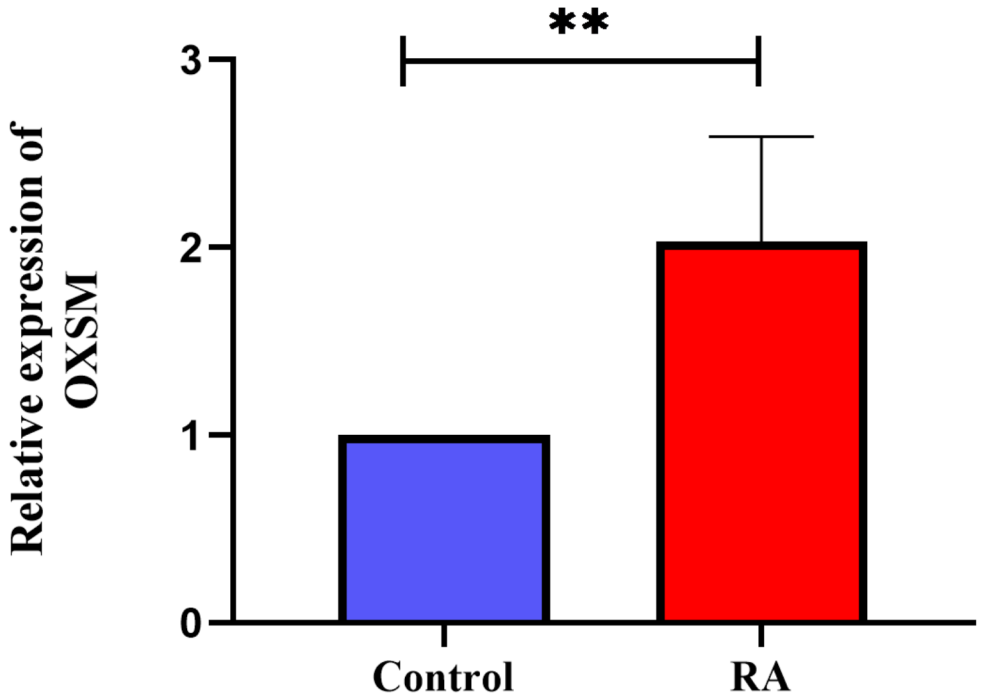

Fig. 17. RT-qPCR results of OXSM expression in rheumatoid arthritis patients and healthy controls.** $P < 0.01$.

To further verify our conclusions, we collected peripheral blood from three healthy controls and five RA patients and measured the relative mRNA expression levels via RT-qPCR. We found that OXSM expression was higher in the RA group than in the control group (Fig. 17A), which is consistent with the results of our bioinformatics analysis(Figs. 5B and 7A). Although, rheumatoid factor (RF) and anti-cyclic citrullinated peptide antibodies (ACPA) were used as the serum biomarkers for the early diagnosis of RA[131,132]. However, both serum markers are not positive in all early RA patients and will have reduced sensitivity, especially when applied to the seronegative patient population[133]. Our results suggest that the OXSM gene may be involved in the pathological process of RA. OXSM as a novel biomarker may be important for the early diagnosis and effective treatment of seronegative patients or RA. Finally, our results will provide new insights into the role of disulfidptosis in RA and identify OXSM potentially as a potential biomarker and target for diagnosing and treating RA.

Undeniably, there are some limitations in our study. First, we should expand the sample size and include a more diverse sample population to validate the specificity and validity of OXSM as a biomarker for diagnosing RA. Secondly, more accurate experiments should be conducted, such as surface plasmon resonance (SPR) to confirm that ICG 001 indeed treats RA through OXSM. Finally, it is necessary to combine animal models or clinical trials to demonstrate the efficacy and safety of ICG 001 in treating RA. Although we are currently limited by resources and time, and have only conducted basic experiments, these will be the focus of our next stage of research.

Conclusion

We identified OXSM as an essential gene associated with disulfidptosis in RA. We established a novel diagnostic model based on OXSM. We verified that OXSM was significantly highly expressed in the peripheral blood of RA patients by RT-qPCR, and OXSM may become a novel biomarker for diagnosing RA. Our findings may improve the accuracy and reliability of diagnostic RA, helping to provide more personalized and effective medical intervention for patients in the future. In addition to its strong association with disulfidptosis, OXSM is also associated with the immune microenvironment in RA patients. At the same time, we also predicted potential drugs targeting OXSM for RA, and molecular docking and molecular dynamics simulations suggested that OXSM and ICG 001 may be potential targets and drugs for treating RA. This is the first study to analyze the relationship between disulfidptosis and RA comprehensively. Although more mechanisms between RA and disulfidptosis have not been elaborated, disulfidptosis may become a future research hotspot for RA treatment.

Data availability

The GSE93272 and GSE45291 datasets used in this study were downloaded from the Gene Expression Omnibus (GEO)(https://www.ncbi.nlm.nih.gov/geo/). The software/package used in this study can be found in the Sange rbox platform (http://vip.sangerbox.com/home.html).

Received: 10 October 2024; Accepted: 7 March 2025
Published online: 13 March 2025

References

1. Smolen, J. S., Aletaha, D. & McInnes, I. B. Rheumatoid arthritis. *Lancet* **388**, 2023–2038 (2016).
2. Komatsu, N. & Takayanagi, H. Mechanisms of joint destruction in rheumatoid arthritis - immune cell-fibroblast-bone interactions. *Nat. Rev. Rheumatol.* **18**, 415–429 (2022).
3. Pirmardvand Chegini, S., Varshosaz, J. & Taymouri, S. Recent approaches for targeted drug delivery in rheumatoid arthritis diagnosis and treatment. *Artif. Cells Nanomed. Biotechnol.* **46**, 502–514 (2018).
4. Zhao, H., Tang, C., Wang, M., Zhao, H. & Zhu, Y. Ferroptosis as an emerging target in rheumatoid arthritis. *Front. Immunol.* **14**, 1260839 (2023).
5. Polat, Y. H. et al. Evaluation of thiol/disulfide homeostasis in rheumatoid arthritis and disease activity. *Clin. Biochem.* **111**, 81–86 (2023).
6. Alisik, M. et al. Erythrocyte reduced/oxidized glutathione and serum thiol/disulfide homeostasis in patients with rheumatoid arthritis. *Clin. Biochem.* **94**, 56–61 (2021).
7. Kaur, G., Sharma, A. & Bhatnagar, A. Role of oxidative stress in pathophysiology of rheumatoid arthritis: insights into NRF2-KEAP1 signalling. *Autoimmunity* **54**, 385–397 (2021).
8. da Fonseca, L. J. S., Nunes-Souza, V., Goulart, M. O. F. & Rabelo, L. A. Oxidative Stress in Rheumatoid Arthritis: What the Future Might Hold regarding Novel Biomarkers and Add-On Therapies. *Oxid Med Cell Longev*. 7536805 (2019). (2019).
9. Phull, A. R., Nasir, B., Haq, I. U. & Kim, S. J. Oxidative stress, consequences and ROS mediated cellular signaling in rheumatoid arthritis. *Chem. Biol. Interact.* **281**, 121–136 (2018).
10. Sakata, S., Kunimatsu, R. & Tanimoto, K. Protective effect of ergothioneine against oxidative Stress-Induced chondrocyte death. *Antioxidants (Basel).* **13**, 800 (2024).
11. Chen, T. et al. Curcumin ameliorates IL-1β-induced apoptosis by activating autophagy and inhibiting the NF-κB signaling pathway in rat primary articular chondrocytes. *Cell. Biol. Int.* **45**, 976–988 (2021).
12. Behl, T. et al. Polyphenols Targeting MAPK Mediated Oxidative Stress and Inflammation in Rheumatoid Arthritis. *Molecules*. 26 (2021).
13. Veale, D. J., Orr, C. & Fearon, U. Cellular and molecular perspectives in rheumatoid arthritis. *Semin Immunopathol.* **39**, 343–354 (2017).
14. Thieblemont, N., Wright, H. L. & Edwards, S. W. Witko-Sarsat, V. Human neutrophils in auto-immunity. *Semin Immunol.* **28**, 159–173 (2016).
15. Dogru, A., Nazıroglu, M. & Cig, B. Modulator role of Infliximab and methotrexate through the transient receptor potential melastatin 2 (TRPM2) channel in neutrophils of patients with rheumatoid arthritis: a pilot study. *Arch. Med. Sci.* **15**, 1415–1424 (2019).
16. Moon, J. S. et al. Cytotoxic CD8(+) T cells target citrullinated antigens in rheumatoid arthritis. *Nat. Commun.* **14**, 319 (2023).
17. Zhang, Y. et al. Microenvironment-Activatable probe for precise NIR-II monitoring and synergistic immunotherapy in rheumatoid arthritis. *Adv. Mater.* **36**, e2409661 (2024).
18. Sarmiento-Salinas, F. L. et al. Reactive oxygen species: role in carcinogenesis, cancer cell signaling and tumor progression. *Life Sci.* **284**, 119942 (2021).
19. Liu, X. et al. Actin cytoskeleton vulnerability to disulfide stress mediates Disulfidptosis. *Nat. Cell. Biol.* **25**, 404–414 (2023).
20. Kuettner, K. E., Aydelotte, M. B. & Thonar, E. J. Articular cartilage matrix and structure: a minireview. *J. Rheumatol. Suppl.* **27**, 46–48 (1991).
21. Lauer, J. C., Selig, M., Hart, M. L., Kurz, B. & Rolauffs, B. Articular chondrocyte phenotype regulation through the cytoskeleton and the signaling processes that originate from or converge on the cytoskeleton: towards a novel Understanding of the intersection between actin dynamics and chondrogenic function. *Int J Mol Sci.* **22**, 3279 (2021).
22. Ciurtin, C. et al. Correlation between different components of synovial fluid and pathogenesis of rheumatic diseases. *Rom J. Intern. Med.* **44**, 171–181 (2006).
23. Steinz, M. M. et al. Oxidative hotspots on actin promote skeletal muscle weakness in rheumatoid arthritis. *JCI Insight.* **5**, e126347 (2019).
24. Vasilopoulos, Y., Gkretsi, V., Armaka, M., Aidinis, V. & Kollias, G. Actin cytoskeleton dynamics linked to synovial fibroblast activation as a novel pathogenic principle in TNF-driven arthritis. *Ann. Rheum. Dis.* **66** (Suppl 3), iii23–28 (2007).
25. Tuzcu, A. et al. Thiol/Disulfide homeostasis in patients with rheumatoid arthritis. *Rom J. Intern. Med.* **57**, 30–36 (2019).
26. Giustarini, D. et al. Altered thiol pattern in plasma of subjects affected by rheumatoid arthritis. *Clin. Exp. Rheumatol.* **23**, 205–212 (2005).
27. Lemarechal, H. et al. High redox thioredoxin but low thioredoxin reductase activities in the serum of patients with rheumatoid arthritis. *Clin. Chim. Acta*. **367**, 156–161 (2006).
28. Wei, K., Nguyen, H. N. & Brenner, M. B. Fibroblast pathology in inflammatory diseases. *J Clin Invest.* **131**, e149538 (2021).
29. Soszyński, M. & Bartosz, G. Decrease in accessible thiols as an index of oxidative damage to membrane proteins. *Free Radic Biol. Med.* **23**, 463–469 (1997).
30. Staroń, A., Mąkosa, G. & Koter-Michalak, M. Oxidative stress in erythrocytes from patients with rheumatoid arthritis. *Rheumatol. Int.* **32**, 331–334 (2012).
31. Chen, J. et al. Disulfidptosis decoded: a journey through cell death mysteries, regulatory networks, disease paradigms and future directions. *Biomark. Res.* **12**, 45 (2024).
32. Xiao, F. et al. Disulfidptosis: A new type of cell death. *Apoptosis*. **29**, 1309–1329 (2024).
33. Ma, S., Wang, D. & Xie, D. Identification of disulfidptosis-related genes and subgroups in Alzheimer's disease. *Front. Aging Neurosci.* **15**, 1236490 (2023).
34. Li, L. et al. Regulation mechanisms of disulfidptosis-related genes in ankylosing spondylitis and inflammatory bowel disease. *Front. Immunol.* **15**, 1326354 (2024).
35. Li, H. et al. Identification of NETs-related biomarkers and molecular clusters in systemic lupus erythematosus. *Front. Immunol.* **14**, 1150828 (2023).
36. Wang, Z. et al. Extraction and analysis of signatures from the gene expression omnibus by the crowd. *Nat. Commun.* **7**, 12846 (2016).
37. Zhou, Y. et al. Identification of copper death-associated molecular clusters and immunological profiles in rheumatoid arthritis. *Front. Immunol.* **14**, 1103509 (2023).
38. Li, A. et al. Identification of SLAMF1 as an immune-related key gene associated with rheumatoid arthritis and verified in mice collagen-induced arthritis model. *Front. Immunol.* **13**, 961129 (2022).
39. Ritchie, M. E. et al. Limma powers differential expression analyses for RNA-sequencing and microarray studies. *Nucleic Acids Res.* **43**, e47 (2015).
40. Hassani, B. et al. Expression analysis of long Non-Coding RNAs related with FOXM1, GATA3, FOXA1 and ESR1 in breast tissues. *Front. Oncol.* **11**, 671418 (2021).

41. Xie, B. et al. Exploring the tumor micro-environment in primary and metastatic tumors of different ovarian cancer histotypes. *Front. Cell. Dev. Biol.* **11**, 1297219 (2023).
42. Kanehisa, M., Furumichi, M., Sato, Y., Kawashima, M. & Ishiguro-Watanabe M. KEGG for taxonomy-based analysis of pathways and genomes. *Nucleic Acids Res.* **51**, D587–d592 (2023).
43. Zhang, Y. et al. Identification of hub genes in colorectal cancer based on weighted gene co-expression network analysis and clinical data from the Cancer genome atlas. *Biosci Rep.* **41**, BSR20211280 (2021).
44. Chen, L. et al. Prediction and analysis of essential genes using the enrichments of gene ontology and KEGG pathways. *PLoS One.* **12**, e0184129 (2017).
45. Langfelder, P. & Horvath, S. WGCNA: an R package for weighted correlation network analysis. *BMC Bioinform.* **9**, 559 (2008).
46. Zhou, N. et al. FerrDb V2: update of the manually curated database of ferroptosis regulators and ferroptosis-disease associations. *Nucleic Acids Res.* **51**, D571–d582 (2023).
47. Liu, Z. et al. Identification of the ferroptosis regulator HELLS with prognostic value for adrenocortical carcinoma based on integrated analysis and experimental validation. *Gland Surg.* **12**, 1251–1270 (2023).
48. Wang, B. et al. Ferroptosis-related biomarkers for Alzheimer's disease: identification by bioinformatic analysis in hippocampus. *Front. Cell. Neurosci.* **16**, 1023947 (2022).
49. Zhu, J., Wu, Y., Ge, X., Chen, X. & Mei, Q. Discovery and validation of Ferroptosis-Associated genes of ulcerative colitis. *J. Inflamm. Res.* **17**, 4467–4482 (2024).
50. Çorbacıoğlu, Ş., Aksel, G. & K. & Receiver operating characteristic curve analysis in diagnostic accuracy studies: A guide to interpreting the area under the curve value. *Turk. J. Emerg. Med.* **23**, 195–198 (2023).
51. Zhou, S., Lu, H. & Xiong, M. Identifying immune cell infiltration and effective diagnostic biomarkers in rheumatoid arthritis by bioinformatics analysis. *Front. Immunol.* **12**, 726747 (2021).
52. Newman, A. M. et al. Robust enumeration of cell subsets from tissue expression profiles. *Nat. Methods.* **12**, 453–457 (2015).
53. Chen, B., Khodadoust, M. S., Liu, C. L., Newman, A. M. & Alizadeh, A. A. Profiling tumor infiltrating immune cells with CIBERSORT. *Methods Mol. Biol.* **1711**, 243–259 (2018).
54. Wang, L. et al. Cuproptosis related genes associated with Jab1 shapes tumor microenvironment and Pharmacological profile in nasopharyngeal carcinoma. *Front. Immunol.* **13**, 989286 (2022).
55. Zhou, G. et al. NetworkAnalyst 3.0: a visual analytics platform for comprehensive gene expression profiling and meta-analysis. *Nucleic Acids Res.* **47**, W234–w241 (2019).
56. Davis, A. P. et al. Comparative toxicogenomics database (CTD): update 2023. *Nucleic Acids Res.* **51**, D1257–d1262 (2023).
57. Liu, Y. et al. CB-Dock2: improved protein-ligand blind Docking by integrating cavity detection, Docking and homologous template fitting. *Nucleic Acids Res.* **50**, W159–w164 (2022).
58. Abraham, M. J. et al. High performance molecular simulations through multi-level parallelism from laptops to supercomputers. *SoftwareX* **GROMACS**, 19–25 (2015).
59. Kalsi, N., Gopalakrishnan, C., Rajendran, V. & Purohit, R. Biophysical aspect of phosphatidylinositol 3-kinase and role of oncogenic mutants (E542K & E545K). *J. Biomol. Struct. Dyn.* **34**, 2711–2721 (2016).
60. Singh, R., Bhardwaj, V. K. & Purohit, R. Inhibition of nonstructural protein 15 of SARS-CoV-2 by golden Spice: A computational insight. *Cell. Biochem. Funct.* **40**, 926–934 (2022).
61. Kalin, S. & Comert Onder, F. Discovery of potential RSK1 inhibitors for cancer therapy using virtual screening, molecular docking, molecular dynamics simulation, and MM/GBSA calculations. *J Biomol Struct Dyn.* **43**, 1424–1444 (2025).
62. Xu, B., Sun, G. & Zhang, Y. Integrated bioinformatics, network pharmacology, molecular docking, and molecular dynamics simulation to explore the potential Pharmacological mechanism of Erigeron breviscapus (Vant.) Hand-Mazz regulating ferroptosis for the treatment of Alzheimer's disease. *J. Mol. Struct.* **1314**, 138698 (2024).
63. Bhardwaj, V. K. & Purohit, R. A comparative study on inclusion complex formation between Formononetin and β-cyclodextrin derivatives through multiscale classical and umbrella sampling simulations. *Carbohydr. Polym.* **310**, 120729 (2023).
64. Hou, T., Wang, J., Li, Y. & Wang, W. Assessing the performance of the MM/PBSA and MM/GBSA methods. 1. The accuracy of binding free energy calculations based on molecular dynamics simulations. *J. Chem. Inf. Model.* **51**, 69–82 (2011).
65. Rastelli, G., Del Rio, A., Degliesposti, G. & Sgobba, M. Fast and accurate predictions of binding free energies using MM-PBSA and MM-GBSA. *J. Comput. Chem.* **31**, 797–810 (2010).
66. Singh, R. & Purohit, R. Computational analysis of protein-ligand interaction by targeting a cell cycle restrainer. *Comput. Methods Programs Biomed.* **231**, 107367 (2023).
67. Bhardwaj, V., Singh, R., Singh, P., Purohit, R. & Kumar, S. Elimination of bitter-off taste of stevioside through structure modification and computational interventions. *J. Theor. Biol.* **486**, 110094 (2020).
68. Zhang, B. & Horvath, S. A general framework for weighted gene co-expression network analysis. *Stat. Appl. Genet. Mol. Biol.* **4**, Article17 (2005).
69. Langfelder, P. & Horvath, S. Eigengene networks for studying the relationships between co-expression modules. *BMC Syst. Biol.* **1**, 54 (2007).
70. Cui, M. et al. Identification of important modules and biomarkers in diabetic cardiomyopathy based on WGCNA and LASSO analysis. *Front. Endocrinol. (Lausanne).* **15**, 1185062 (2024).
71. Petri, M. et al. Association between changes in gene signatures expression and disease activity among patients with systemic lupus erythematosus. *BMC Med. Genomics.* **12**, 4 (2019).
72. Gu, X. et al. Hub genes, diagnostic model, and predicted drugs related to Iron metabolism in Alzheimer's disease. *Front. Aging Neurosci.* **14**, 949083 (2022).
73. Oka, S. et al. Plasma MiRNA expression profiles in rheumatoid arthritis associated interstitial lung disease. *BMC Musculoskelet. Disord.* **18**, 21 (2017).
74. Liu, F., Huang, Y., Liu, F. & Wang, H. Identification of immune-related genes in diagnosing atherosclerosis with rheumatoid arthritis through bioinformatics analysis and machine learning. *Front. Immunol.* **14**, 1126647 (2023).
75. Sekiguchi, Y. et al. Methotrexate-associated hodgkin lymphoma in a patient with rheumatoid arthritis successfully treated with Brentuximab Vedotin in combination with doxorubicin, vinblastine, and Dacarbazine (BV + AVD). *Intern. Med.* **59**, 2165–2171 (2020).
76. Dehlin, M., Andersson, S., Erlandsson, M., Brisslert, M. & Bokarewa, M. Inhibition of fms-like tyrosine kinase 3 alleviates experimental arthritis by reducing formation of dendritic cells and antigen presentation. *J. Leukoc. Biol.* **90**, 811–817 (2011).
77. Chen, X. et al. Schisandrin B ameliorates adjuvant-induced arthritis in rats via modulation of inflammatory mediators, oxidative stress, and HIF-1α/VEGF pathway. *J. Pharm. Pharmacol.* **76**, 681–690 (2024).
78. Saikia, S. & Bordoloi, M. Molecular docking: challenges, advances and its use in drug discovery perspective. *Curr. Drug Targets.* **20**, 501–521 (2019).
79. Duan, H. et al. Exploring the therapeutic mechanisms of gleditsiae spina acting on pancreatic cancer via network pharmacology, molecular Docking and molecular dynamics simulation. *RSC Adv.* **13**, 13971–13984 (2023).
80. Que, W. et al. Molecular mechanism of Gelsemium elegans (Gardner and Champ.) Benth. Against neuropathic pain based on network Pharmacology and experimental evidence. *Front. Pharmacol.* **12**, 792932 (2021).
81. Singh, R., Bhardwaj, V. K., Sharma, J., Das, P. & Purohit, R. Identification of selective cyclin-dependent kinase 2 inhibitor from the library of pyrrolone-fused benzosuberene compounds: an in Silico exploration. *J. Biomol. Struct. Dyn.* **40**, 7693–7701 (2022).

82. Ramachandran, G. N., Ramakrishnan, C. & Sasisekharan, V. Stereochemistry of polypeptide chain configurations. *J. Mol. Biol.* **7**, 95–99 (1963).
83. Ding, Q. et al. Signaling pathways in rheumatoid arthritis: implications for targeted therapy. *Signal. Transduct. Target. Ther.* **8**, 68 (2023).
84. Wu, Y. K., Liu, C. D., Liu, C., Wu, J. & Xie, Z. G. Machine learning and weighted gene co-expression network analysis identify a three-gene signature to diagnose rheumatoid arthritis. *Front. Immunol.* **15**, 1387311 (2024).
85. Hu, K. et al. Identification and construction of a Disulfidptosis-Mediated diagnostic model and associated immune microenvironment of osteoarthritis from the perspective of PPPM. *J. Inflamm. Res.* **17**, 3753–3770 (2024).
86. Hansildaar, R. et al. Cardiovascular risk in inflammatory arthritis: rheumatoid arthritis and gout. *Lancet Rheumatol.* **3**, e58–e70 (2021).
87. He, X. et al. Identification of potential ferroptosis-associated biomarkers in rheumatoid arthritis. *Front. Immunol.* **14**, 1197275 (2023).
88. Fu, M. et al. Identification of key Disulfidptosis-Related genes and their association with gene expression subtypes in Crohn's disease. *J. Inflamm. Res.* **17**, 3655–3670 (2024).
89. Liu, W. et al. Energy competition remodels the metabolic glucose landscape of psoriatic epidermal cells. *Theranostics* **14**, 3339–3357 (2024).
90. Xiong, Z. et al. Exploring the relevance of Disulfidptosis to the pathophysiology of ulcerative colitis by bioinformatics analysis. *J. Inflamm. Res.* **17**, 2757–2774 (2024).
91. Weyand, C. M. & Goronzy, J. J. The immunology of rheumatoid arthritis. *Nat. Immunol.* **22**, 10–18 (2021).
92. Shrivastav, M., Mittal, B., Aggarwal, A. & Misra, R. Autoantibodies against cytoskeletal proteins in rheumatoid arthritis. *Clin. Rheumatol.* **21**, 505–510 (2002).
93. Zhang, L., Joshi, A. K., Hofmann, J., Schweizer, E. & Smith, S. Cloning, expression, and characterization of the human mitochondrial beta-ketoacyl synthase. Complementation of the yeast CEM1 knock-out strain. *J. Biol. Chem.* **280**, 12422–12429 (2005).
94. Nowinski, S. M. et al. Mitochondrial fatty acid synthesis coordinates oxidative metabolism in mammalian mitochondria. *Elife.* **9**, e58041 (2020).
95. Zhang, L., Zhao, S., Liu, Y., Lv, F. & Geng, X. Identification and validation of transcription factor-driven enhancers of genes related to lipid metabolism in metastatic oral squamous cell carcinomas. *BMC Oral Health.* **22**, 126 (2022).
96. Gao, T. et al. Reduction of mitochondrial 3-oxoacyl-ACP synthase (OXSM) by hyperglycemia is associated with deficiency of α-lipoic acid synthetic pathway in kidney of diabetic mice. *Biochem. Biophys. Res. Commun.* **512**, 106–111 (2019).
97. Zhang, D. et al. An integrative multi-omics analysis based on disulfidptosis-related prognostic signature and distinct subtypes of clear cell renal cell carcinoma. *Front. Oncol.* **13**, 1207068 (2023).
98. Šuštić, T., Bosdriesz, E., van Wageningen, S., Wessels, L. F. A. & Bernards, R. RUNX2/CBFB modulates the response to MEK inhibitors through activation of receptor tyrosine kinases in KRAS-mutant colorectal cancer. *Transl Oncol.* **13**, 201–211 (2020).
99. Hu, G. et al. A bioinformatics approach to identify a disulfidptosis-related gene signature for prognostic implication in colon adenocarcinoma. *Sci. Rep.* **13**, 12403 (2023).
100. Duan, Y. et al. Knockdown of heat shock protein family D member 1 (HSPD1) promotes proliferation and migration of ovarian cancer cells via disrupting the stability of mitochondrial 3-oxoacyl-ACP synthase (OXSM). *J. Ovarian Res.* **16**, 81 (2023).
101. Wang, W. Y. & Lu, W. C. Reduced expression of hsa-miR-338-3p contributes to the development of glioma cells by targeting mitochondrial 3-Oxoacyl-ACP synthase (OXSM) in glioblastoma (GBM). *Onco Targets Ther.* **13**, 9513–9523 (2020).
102. Xu, Y., Shen, J. & Ran, Z. Emerging views of mitophagy in immunity and autoimmune diseases. *Autophagy* **16**, 3–17 (2020).
103. Ma, C., Wang, J., Hong, F. & Yang, S. *Mitochondrial Dysfunction in Rheumatoid Arthritis. Biomolecules.* **12**, 1216 (2022).
104. Su, D. et al. (99) Tc-methylene diphosphonate improves rheumatoid arthritis disease activity by increasing the frequency of peripheral γδ T cells and CD4(+) CD25(+) Foxp3(+) Tregs. *Int J Rheum Dis*. 19, 586–593 (2016).
105. Liu, R. & Proud, C. G. Eukaryotic elongation factor 2 kinase as a drug target in cancer, and in cardiovascular and neurodegenerative diseases. *Acta Pharmacol. Sin*. **37**, 285–294 (2016).
106. Bank, I. The Role of Gamma Delta T Cells in Autoimmune Rheumatic Diseases. *Cells*. 9 (2020).
107. Bank, I. & Marcu-Malina, V. Quantitative peripheral blood perturbations of Γδ T cells in human disease and their clinical implications. *Clin. Rev. Allergy Immunol.* **47**, 311–333 (2014).
108. Papotto, P. H., Reinhardt, A., Prinz, I. & Silva-Santos, B. Innately versatile: Γδ17 T cells in inflammatory and autoimmune diseases. *J. Autoimmun.* **87**, 26–37 (2018).
109. Gaur, P., Misra, R. & Aggarwal, A. Natural killer cell and gamma delta T cell alterations in enthesitis related arthritis category of juvenile idiopathic arthritis. *Clin. Immunol.* **161**, 163–169 (2015).
110. Noack, M. & Miossec, P. Th17 and regulatory T cell balance in autoimmune and inflammatory diseases. *Autoimmun. Rev.* **13**, 668–677 (2014).
111. Bilate, A. M. & Lafaille, J. J. Induced CD4 + Foxp3 + regulatory T cells in immune tolerance. *Annu. Rev. Immunol.* **30**, 733–758 (2012).
112. Li, B. et al. Differential immunological profiles in seronegative versus seropositive rheumatoid arthritis: Th17/Treg dysregulation and IL-4. *Front. Immunol.* **15**, 1447213 (2024).
113. Samson, M. et al. Brief report: Inhibition of interleukin-6 function corrects Th17/Treg cell imbalance in patients with rheumatoid arthritis. *Arthritis Rheum.* **64**, 2499–2503 (2012).
114. McInnes, I. B. & Schett, G. The pathogenesis of rheumatoid arthritis. *N Engl. J. Med.* **365**, 2205–2219 (2011).
115. Jiang, Q., Yang, G., Liu, Q., Wang, S. & Cui, D. Function and role of regulatory T cells in rheumatoid arthritis. *Front. Immunol.* **12**, 626193 (2021).
116. Lv, Y. et al. Bioinformatics and systems biology approach to identify the pathogenetic link of long COVID and myalgic encephalomyelitis/chronic fatigue syndrome. *Front. Immunol.* **13**, 952987 (2022).
117. Hobert, O. Gene regulation by transcription factors and MicroRNAs. *Science* **319**, 1785–1786 (2008).
118. Kakan, S. S. et al. Tear MiRNAs identified in a murine model of Sjögren's syndrome as potential diagnostic biomarkers and indicators of disease mechanism. *Front. Immunol.* **13**, 833254 (2022).
119. Chen, D. et al. Up-regulation of urinary Exosomal hsa-microRNA-200b-3p and hsa-microRNA-206 in patients of steroid-induced osteonecrosis of femoral head. *Am. J. Transl Res.* **13**, 7574–7590 (2021).
120. Navarro Quiroz, E. et al. Integrated analysis of MicroRNA regulation and its interaction with mechanisms of epigenetic regulation in the etiology of systemic lupus erythematosus. *PLoS One.* **14**, e0218116 (2019).
121. Alatas, E. T., Kara, M. & Dogan, G. Akın Belli, A. Blood MicroRNA expressions in patients with mild to moderate psoriasis and the relationship between MicroRNAs and psoriasis activity. *Bras. Dermatol.* **95**, 702–707 (2020).
122. Zheng, Q., Wang, D., Lin, R., Lv, Q. & Wang, W. IFI44 is an immune evasion biomarker for SARS-CoV-2 and Staphylococcus aureus infection in patients with RA. *Front. Immunol.* **13**, 1013322 (2022).
123. Henderson, W. R. Jr. et al. Inhibition of Wnt/beta-catenin/CREB binding protein (CBP) signaling reverses pulmonary fibrosis. *Proc. Natl. Acad. Sci. U S A*. **107**, 14309–14314 (2010).
124. Danieau, G. et al. ICG-001, an inhibitor of the β-Catenin and cAMP response Element-Binding protein dependent gene transcription, decreases proliferation but enhances migration of osteosarcoma cells. *Pharmaceuticals (Basel).* **14**, 421 (2021).

125. Liu, Y. et al. ICG-001 suppresses growth of gastric cancer cells and reduces chemoresistance of cancer stem cell-like population. *J. Exp. Clin. Cancer Res.* **36**, 125 (2017).
126. Hsin, I. L. et al. β-catenin inhibitor ICG-001 suppress cell cycle progression and induce autophagy in endometrial cancer cells. *J. Cell. Physiol.* **238**, 2440–2450 (2023).
127. Huang, Y. et al. Wnt/β-catenin inhibitor ICG-001 enhances the antitumor efficacy of radiotherapy by increasing radiation-induced DNA damage and improving tumor immune microenvironment in hepatocellular carcinoma. *Radiother Oncol.* **162**, 34–44 (2021).
128. Bartok, B. & Firestein, G. S. Fibroblast-like synoviocytes: key effector cells in rheumatoid arthritis. *Immunol. Rev.* **233**, 233–255 (2010).
129. Xiao, C. Y. et al. Expression of β-catenin in rheumatoid arthritis fibroblast-like synoviocytes. *Scand. J. Rheumatol.* **40**, 26–33 (2011).
130. Wiese, M. et al. The β-catenin/CBP-antagonist ICG-001 inhibits pediatric glioma tumorigenicity in a Wnt-independent manner. *Oncotarget* **8**, 27300–27313 (2017).
131. Allard-Chamard, H. & Boire, G. Serologic diagnosis of rheumatoid arthritis. *Clin. Lab. Med.* **39**, 525–537 (2019).
132. Cush, J. J. Rheumatoid arthritis: early diagnosis and treatment. *Med. Clin. North. Am.* **105**, 355–365 (2021).
133. Perera, J., Delrosso, C. A., Nerviani, A. & Pitzalis, C. Clinical phenotypes, serological biomarkers, and synovial features defining seropositive and seronegative rheumatoid arthritis: A literature review. *Cells.* **13**, 743 (2024).

Acknowledgements

We thank the GEO database, and the FerrDb database for the analytical data. We also thank Sangerbox for providing us with the platform as part of the data analysis.

Author contributions

BX: Designed and conceived, data analysis, molecular biology experiments, wrote, revised, confirmed final manuscript and provided funds. QG: Collected and processed data, analyzed data, revised the manuscript and confirmed the final draft. XDL: Designed and conceived, data analysis, revised and confirmed the final draft. HLZ: Software operation. BS: Sample collection. JMW: Investigation. MTS: Statistical data analysis. All authors have reviewed and approved the submission of the manuscript.All authors reviewed the manuscript.

Funding

This work was supported by the Science and Technology Fund Project of the Guizhou Provincial Health Commission (No. gzwkj2024–523) and the Science and Technology Program of Anshun City (No. ASKC-2021–12, No. ASKC-2024–17).

Declarations

Competing interests

The authors declare no competing interests.

Ethics statement

The human blood sample collection protocol was approved by the Ethics Committee of Anshun People's Hospital, Guizhou Province. Written informed consent was obtained from all participants before enrollment.

Conflict of interest

The authors declare that the research was conducted in the absence of any commercial or financial relationships that could be construed as a potential conflict of interest.

Additional information

Supplementary Information The online version contains supplementary material available at https://doi.org/10.1038/s41598-025-93656-4.

Correspondence and requests for materials should be addressed to B.X., X.D.L. or Q.G.